4-NODE SEMI-EAS ELEMENT IN 6-FIELD NONLINEAR THEORY OF SHELLS

Journal:	*International Journal for Numerical Methods in Engineering*
Manuscript ID:	NME-Nov-05-0606.R1
Wiley - Manuscript type:	Research Article
Date Submitted by the Author:	15-Feb-2006
Complete List of Authors:	Chróscielewski, Jacek Witkowski, Wojciech
Keywords:	EAS, 6-FIELD SHELL, SHELL INTERSECTION, SO(3), QUADRILATERAL SHELL ELEMENT, LOCKING

4–NODE SEMI-EAS ELEMENT

IN 6–FIELD NONLINEAR THEORY OF SHELLS

J. CHRÓŚCIELEWSKI, W. WITKOWSKI,
GDANSK UNIVERSITY OF TECHNOLOGY,
FACULTY OF CIVIL AND ENVIRONMENTAL ENGINEERING
NARUTOWICZA 11/12
80-952 GDANSK POLAND

CORRESPONDING AUTHOR

GDANSK UNIVERSITY OF TECHNOLOGY,
FACULTY OF CIVIL AND ENVIRONMENTAL ENGINEERING
NARUTOWICZA 11/12
80-952 GDANSK POLAND
PHONE +48 58 347 21 74
FAX +48 58 347 16 70
email wojwit@pg.gda.pl

ACKNOWLEDGEMENTS

The financial support of the Polish State Committee for Scientific Research under Grant No 5 T07 A 00825 is gratefully acknowledged.

Wojciech Witkowski is awarded by Foundation for Polish Science.

ABSTRACT

We propose a new 4–node C^0 finite element for shell structures undergoing unlimited translations and rotations. The considerations concern the general 6–field theory of shells with asymmetric strain measures in geometrically nonlinear static problems. The shell kinematics is of the two-dimensional Cosserat continuum type and is described by two independent fields: the vector field for translations and the proper orthogonal tensor field for rotations. All three rotational parameters are treated here as independent. Hence, as a consequence of the shell theory, the proposed element has naturally six engineering degrees of freedom at each node, with the so-called drilling rotation. This property makes the element suitable for analysis of shell structures containing folds, branches or intersections. To avoid locking phenomena we use the Enhanced Assumed Strain (EAS) concept. We derive and linearize the modified Hu-Washizu principle for 6–field theory of shells. What makes the present approach original is the combination of EAS method with asymmetric membrane strain measures. Based on literature, we propose new enhancing field and specify the transformation matrix that accounts for the lack of symmetry. To gain knowledge about the suitability of this field for asymmetric strain measures and to assess the performance of the element, we solve typical benchmark examples with smooth geometry and examples involving orthogonal intersections of shell branches.

KEYWORDS: EAS, LOCKING, 6–PARAMETER SHELL, SO(3), QUADRILATERAL SHELL ELEMENT, SHELL INTERSECTIONS

1. INTRODUCTION

We present a formulation of the new 4–node C^0 nonlinear shell finite element. The essential feature of the formulation is the employed theory of shells, which is

statically and kinematically exact. Hence, kinematical hypotheses such as that of Reissner-Mindlin type are not introduced here. The kinematics of the shell is described by the field of generalized displacements, composed of the translation field and the rotation field that appear naturally as independent variables. Being a kinematically exact, the present shell theory accommodates finite (unlimited) translations and rotations. The presence of rotation tensor causes that the sixth degree of freedom appears naturally at each node of FEM mesh. Thus, the elaborated shell element is well suited for analysis of shell structures containing intersections. To avoid the well-known locking effect, we use the Enhanced Assumed Strain (EAS) concept to enhance the stretching strains (including also the shearing components). The bending strains are not enhanced. Thus, we regard the proposed finite element as semi-enhanced. The element is elaborated in the stationary Lagrangian formulation from the modified Hu–Washizu variational principle with generalized displacements and asymmetric membrane strains. Based on the literature we propose an enhancing field taking into account the asymmetric membrane strains. Such formulation combining asymmetric strain measures with EAS technique, to the best of the authors' knowledge, has not been attempted before.

In the literature, nowadays two trends may be distinguished in formulation of shell elements: the degenerated shell element (e.g. [1], [2], [3], [4]) and the Reissner-Mindlin type shell element. The latter approach has been extensively studied by J.C. Simo and his co-workers who proposed modern and mathematically elegant formulation of Reissner-Mindlin theory. In particular, they paid a special attention to the rotation tensor. In a series of papers, see for example, [5] a complete theory and finite elements were formulated. However, in [6] it has been shown that these both approaches have the same foundations: they require only C^0 continuity and in classical formulation, they stem from the kinematical

assumption saying that fibers along the thickness remain straight and inextensible. When combined with FEM discretization both the above approaches lead to elements with five degrees of freedom per node: three translations and two parameters of rotations. Hence, an inconvenience appears when these elements are to be applied to structures of which geometry contains irregularities such as, for instance, orthogonal intersections of elements.

Another way of formulating shell elements is to develop them from such theory of shells where all six degrees of freedom (including the rotation normal to the reference surface) appear on the level of mathematical formulation, see for instance [7], [8], [9], [10] or [11]. In this paper, we employ as a point of departure the general nonlinear theory of shells firstly proposed by Reissner [12] and developed by Libai and Simmonds [13]. The main features of the underlying theory of shells may be recapitulated after [14]-[17] as follows:

a. The shell (or the shell-like body) is an ordinary material continuum merely of specific geometry. Thus, the motion and deformation of the shell are described by general balance laws of solid mechanics.
b. The shell-like body is represented by a base surface endowed with mechanical properties and internal structure.
c. The shell theory is statically exact: the exact two-dimensional equilibrium equations of the shell-like body are derived by direct through-the thickness integration from three-dimensional balance laws of linear and angular momentum. The equilibrium equations are expressed in terms of resultant quantities. Therefore, from the computational viewpoint there is no necessity of integration over the element volume, typical for the degenerated elements.
d. The shell theory is kinematically exact: the shell kinematics is a direct implication of an integral identity resulting from the exact equilibrium equations derived as specified

above in (c). The resulting kinematic model is formally equivalent to the Cosserat surface. The so-called drilling dof is the natural consequence of the theoretical shell model.

e. The (virtual) two-dimensional strain measures - the stretching and the bending vectors - are implied again by the integral identity. As work-conjugate to the stress and couple resultants, the strain measures are the most natural ones.

f. The whole shell theory is so formulated that the only approximate feature of the underlying theory of results from the use of two-dimensional constitutive laws.

The present theory allows for unlimited translations and rotations and it accommodates naturally various geometric irregularities such as, for example, folds, branches and/or intersections. If these effects are to be considered, there arises a necessity to add suitable jump conditions to the theoretical formulation. Due to the main aim of the paper we do not discuss these issues here, for details see [16].

The computational aspects within the framework of this theory of shells were already covered in [14] where families of 4-, 9- and 16-node displacement/rotation finite elements named CAM were elaborated. Later in [15] and [16] mixed and Assumed Natural Strain (ANS technique, according to [18]) elements were developed. The summary and the recent advances within this shell theory and its numerical implementation may be found in the book [17]. Hence, the EAS element proposed here completes naturally the families of shell elements developed in [14]-[16].

The EAS elements stem from the so-called modified Hu-Washizu variational principle, with appropriate energy-conjugate strain and stress measures. Originally (cf. [19]), these elements were classified as hybrid-mixed elements. However, Braess [20] showed that EAS formulation should be rather viewed as “softened” displacement model, due to the structure of weak formulation and resulting forms of the element matrices.

Therefore, in this paper we make an extensive use of the results obtained in [14]-[17] with regard to the displacement/rotation elements. However, the novelty of the present study, in comparison with [14]-[17], stems from the application of the (EAS) technique used as a remedy for the locking effect.

Application of EAS concept, or of method of incompatible modes (cf. [21]) in formulation of shell elements is already well-known in the literature, see for example [2], [3], [4], [9], [22], [23] or [24], to name but a few papers. What makes the present paper original is the combination of the semi-EAS concept with asymmetric strain measures that are inherent to the general theory of shells. Additionally, following [3] we apply here the EAS technique uniformly to all components of the stretching strain vector. This is different from approach utilized in, for example [2], [22], [23] where the combined elements were elaborated i.e.: EAS technique used for membrane strains and ANS technique for shear strains.

The present paper is organised as follows. Firstly, we discuss the main necessary features of the underlying shell theory in Section 2. Section 3 is devoted to two-dimensional kinematics of the shell. Attention is paid to definition of strain measures and their virtual counterparts. Furthermore, the constitutive relations are discussed. Sections 4 and 5 are concerned with FEM interpolation, discretization and formulation of EAS elements. Special attention is devoted to interpolation on the $SO(3)$ group. Based on the existing literature we propose the enhancing field for asymmetric strain measures. In Section 6 we briefly discuss the exact update procedure. In Section 7, the element is subjected to tests. This section is divided into two parts. The first one comprises benchmark problems with smooth geometry. In the second part, the examples contain orthogonal intersections of shell branches, thereby it is possible to ascertain that the implemented enhancing field is properly chosen for the

theory of shells with the drilling rotation. In both parts of Section 7 the considerations are confined to linear elastic thin isotropic shells in static problems.

2. GOVERNING EQUATIONS

In this section, main aspects of the underlying theory of shells are covered in the range necessary for FEM implementation. We refer to [14]-[17] for more detailed formulation.

As mentioned above a shell is a three-dimensional solid body B with specific geometry (see Fig. 1). We assume that the boundary ∂B of B is a union of three parts: the upper surface M^+, the lower surface M^- and the lateral surface $\partial B'$ (see Fig. 1). M denotes the base surface of the shell (which must not be necessarily the middle surface). The boundary ∂M of M is a union of two parts $\partial M = \partial M_d \cup \partial M_f$ on which the displacement (∂M_d) and the traction (∂M_f) boundary conditions are imposed respectively. We also assume that upper and lower surfaces do not have any common points, i.e.

$$\partial B = M^+ \cup M^- \cup \partial B', \qquad M^+ \cap M^- = \varnothing. \tag{2.1}$$

For the so defined shell, three main principles of mechanics must be satisfied: the conservation of mass, the conservation of linear momentum and the conservation of angular momentum. In static problems, the principle of mass conservation is satisfied identically and is not considered directly here. Two latter principles specify respectively to global equilibrium equations of forces and torques, defined below.

Let B be a reference configuration of the shell-like body and P be a selected but arbitrary part of B (see Fig. 2). Here $P \subset B$ is defined by surfaces Π^+, Π^- and $\partial P'$. Therefore, $\partial P'$ cuts out from M a bounded region Π (see Fig.2) where $\boldsymbol{\nu}$ is the

outward unit vector normal to $\partial\Pi$. When recast into the two-dimensional formulation, the equations of equilibrium of forces and torques take the following forms (see for instance [14] and [16]):

$$\begin{aligned} \iint_{\Pi} \boldsymbol{f} da + \int_{\partial\Pi\setminus\partial M_f} \boldsymbol{n_v} dl + \int_{\partial\Pi\cap\partial M_f} \boldsymbol{n}^* dl = \boldsymbol{0} \\ \iint_{\Pi} (\boldsymbol{c} + \boldsymbol{y}\times\boldsymbol{f}) da + \int_{\partial\Pi\setminus\partial M_f} (\boldsymbol{m_v} + \boldsymbol{y}\times\boldsymbol{n_v}) dl + \int_{\partial\Pi\cap\partial M_f} (\boldsymbol{m}^* + \boldsymbol{y}\times\boldsymbol{n}^*) dl = \boldsymbol{0}. \end{aligned} \tag{2.2}$$

These two equations hold for every part $\Pi \subset M$ (see Fig. 3). In (2.2) $\boldsymbol{f}(\boldsymbol{x})$ and $\boldsymbol{c}(\boldsymbol{x})$ are the resultant surface force vector and the resultant surface couple vector, respectively, $\boldsymbol{y}$ denotes the position vector of the base surface of the shell in the deformed configuration.

The local equations of equilibrium are formulated in the following steps. Let $\boldsymbol{n_v}$ and $\boldsymbol{m_v}$ be the resultant stress and the resultant stress couple vectors defined along each smooth internal curve $\partial\Pi \in M$, and $\boldsymbol{n}*$ and $\boldsymbol{m}*$ be the given boundary resultant tractions and moments, respectively (see Fig. 3). Upon applying now the Stokes theorem to (2.2), the local equations of equilibrium take the form:

$$\boldsymbol{n}^{\beta}{}_{|\beta} + \boldsymbol{f} = \boldsymbol{0}, \quad \boldsymbol{m}^{\beta}{}_{|\beta} + \boldsymbol{y}_{,\beta}\times\boldsymbol{n}^{\beta}{}_{|\beta} + \boldsymbol{c} = \boldsymbol{0}, \tag{2.3}$$

$$\boldsymbol{n_v} = \boldsymbol{n}^{\beta}\nu_{\beta}, \quad \boldsymbol{m_v} = \boldsymbol{m}^{\beta}\nu_{\beta}. \tag{2.4}$$

The above equations hold for every regular point of M. In (2.3) $(.)_{|\beta}$ denotes the covariant derivative in the metric of the reference base surface M, which classifies the present development as the Lagrangian-type formulation. In the above equations $\beta = 1,2$ correspond to a two-dimensional local parametrization of M.

For the completeness, the equations (2.3) are supplemented with the mechanical (static) boundary conditions

$$\boldsymbol{n}^{\beta}\nu_{\beta} = \boldsymbol{n}*, \quad \boldsymbol{m}^{\beta}\nu_{\beta} = \boldsymbol{m}*. \tag{2.5}$$

For computational purposes, we assume now that the undeformed base surface M is parametrized by arc-length coordinates $\boldsymbol{s} = (s_1, s_2)$ with associated unit vectors $\boldsymbol{t}_\beta^0$ tangent to M and a normal vector $\boldsymbol{t}^0$ (see Fig. 4). Formally, these vectors are defined by

$$\boldsymbol{t}_\beta^0 = \frac{\partial \boldsymbol{x}}{\partial s_\beta}, \qquad \boldsymbol{t}^0 \equiv \boldsymbol{t}_3^0, \qquad (\boldsymbol{t}_1^0 \times \boldsymbol{t}_2^0) \cdot \boldsymbol{t}^0 > 0 . \tag{2.6}$$

Notation $(2.6)_1$ is purely formal, for from the computational viewpoint the triad $\{\boldsymbol{t}_i^0\}$ and $\boldsymbol{x}$ describing geometry of M are treated as a part of input data of the problem (see Fig. 4). At each regular point of M $\{\boldsymbol{t}_i^0\}$ is defined as a transformation of some global fixed base $\{\mathbf{e}_i\}$

$$\boldsymbol{t}_i^0(\boldsymbol{x}) = \boldsymbol{T}_0(\boldsymbol{x})\mathbf{e}_i, \qquad \boldsymbol{T}_0(\boldsymbol{x}) = \boldsymbol{t}_i^0(\boldsymbol{x}) \otimes \mathbf{e}_i, \qquad i = 1,2,3 . \tag{2.7}$$

Here $\boldsymbol{T}_0$ is referred to as the tensor of structure of the shell in the reference configuration. In the FEM approach the most suitable way is to assume the triad to be orthonormal, i.e.

$$\boldsymbol{t}_i^0 \cdot \boldsymbol{t}_j^0 = \delta_{ij}, \qquad \boldsymbol{t}_i^0 = \boldsymbol{t}_0^i, \qquad \boldsymbol{t}^0 \equiv \boldsymbol{t}_0^3, \qquad \| \boldsymbol{t}_i^0 \| = 1 , \tag{2.8}$$

although there is no necessity to do so. Upon this assumption $\boldsymbol{T}_0$ becomes a member of the proper rotation group, $\boldsymbol{T}_0 \in SO(3)$. Then (2.7) describes rotation of the basis $\{\mathbf{e}_i\}$ to $\{\boldsymbol{t}_i^0\}$ and $\boldsymbol{T}_0$ may be expressed in matrix form in the base $\{\mathbf{e}_i\}$ as

$$\mathbf{T}_0(\boldsymbol{x}) \equiv [\mathbf{t}_1^0(\boldsymbol{x}) \,|\, \mathbf{t}_2^0(\boldsymbol{x}) \,|\, \mathbf{t}_3^0(\boldsymbol{x})] . \tag{2.9}$$

It should be noticed that the equations (2.2) are straightforward implication of three-dimensional balance laws of continuum mechanics. In this sense they are exact. Furthermore, these equations are obtained without resorting to any simplifying assumptions so often used in the literature in the context of various shell formulations,

e.g. about the magnitude of displacements or rotations, or the kinematical hypotheses of the Kirchhoff-Love or Reissner-Mindlin type. In particular, there is no even reference here to the shell thickness. Therefore, the above formulation holds for any shell-like shell and is independent of material composing the body in question.

The explicit appearance of variables from the rotation group $SO(3)$ requires precise treatment of operations, since this group is multiplicative. This issue has already received a major attention in the literature. For instance, references [25], [26] are devoted to the general problems, in [27], [28], [29] beam problems are discussed and references [17] and [30] are concerned shells. This list is far from being complete, yet these papers give a decent view into the subject. Appendix 1 of this paper summarizes some of the facts concerning rotations that are employed here.

3. KINEMATICS OF SHELL

Let us assume that $\boldsymbol{v}(\boldsymbol{x})$ and $\boldsymbol{w}(\boldsymbol{x})$ are: the kinematically admissible displacement field and the kinematically admissible rotation field respectively. These fields have to satisfy the homogenous boundary conditions $\boldsymbol{v}(\boldsymbol{x}) = \boldsymbol{0}$, $\boldsymbol{w}(\boldsymbol{x}) = \boldsymbol{0}$ on ∂M_d. Then the following calculations can be performed. Firstly, the scalar products of $(2.3)_1$ with $\boldsymbol{v}(\boldsymbol{x})$ and $(2.3)_2$ with $\boldsymbol{w}(\boldsymbol{x})$ are computed. Secondly, the resulting expressions are summed and integrated over M. Thirdly, to the obtained expression the Stokes theorem is applied yielding the following integral identity

$$G_i(M;\mathbf{W}) = G_e(M;\mathbf{W}), \qquad \mathbf{W} \equiv (\boldsymbol{v},\boldsymbol{w}), \tag{3.1}$$

where

$$\begin{aligned} G_i(M;\mathbf{W}) &\equiv \iint_M \{\boldsymbol{n}^{\beta}{}_{|\beta} \cdot (\boldsymbol{v}_{,\beta} + \boldsymbol{y}_{,\beta} \times \boldsymbol{w}) + \boldsymbol{m}^{\beta}{}_{|\beta} \cdot \boldsymbol{w}_{,\beta}\} da, \\ G_e(M;\mathbf{W}) &\equiv \iint_M (\boldsymbol{f} \cdot \boldsymbol{v} + \boldsymbol{c} \cdot \boldsymbol{w}) da + \int_{\partial M_f} (\boldsymbol{n}^{*} \cdot \boldsymbol{v} + \boldsymbol{m}^{*} \cdot \boldsymbol{w}) dl. \end{aligned} \tag{3.2}$$

Since $G_e(M;\mathbf{w})$ has clear meaning of the work done by external loads, then by (3.1) the term $G_i(M;\mathbf{w})$ is the virtual work of internal forces. It may be argued (see [14]) that the terms

$$\delta\boldsymbol{\varepsilon}_\beta = \boldsymbol{v}_{,\beta} + \boldsymbol{y}_{,\beta}\times\boldsymbol{w} \tag{3.3}$$

and

$$\boldsymbol{\kappa}_\beta = \boldsymbol{w}_{,\beta} \tag{3.4}$$

should be viewed as virtual changes of some kind of strain measures. The studies of Reissner [12] and Simmonds [31] pointed out that the kinematical model associated with (3.2) is identical to the Cosserat surface.

Typically, in the spatial representation, the configuration of the Cosserat surface model is described by two fields

$$\boldsymbol{y}(\boldsymbol{x},t) = \boldsymbol{x} + \boldsymbol{u}(\boldsymbol{x},t), \quad \boldsymbol{T}(\boldsymbol{x},t) = \boldsymbol{Q}(\boldsymbol{x},t)\boldsymbol{T}_0(\boldsymbol{x}), \tag{3.5}$$

where $\boldsymbol{y}$ is defined in (2.2), $\boldsymbol{u}$ is the displacement vector, and t parametrizes a smooth curve on the configuration space. $\boldsymbol{T}(\boldsymbol{x},t)\in SO(3)$ is the so-called tensor of structure of the shell in the current (deformed) configuration. The tensor $\boldsymbol{T}(\boldsymbol{x},t)$ may be viewed as an image of $\boldsymbol{T}_0\in SO(3)$ under action of the rotation tensor $\boldsymbol{Q}\in SO(3)$. Therefore, based on relation (2.7) we have

$$\boldsymbol{t}_i(\boldsymbol{x}) = \boldsymbol{Q}(\boldsymbol{x})\boldsymbol{t}_i^0(\boldsymbol{x}) = \boldsymbol{Q}(\boldsymbol{x})\boldsymbol{T}_0(\boldsymbol{x})\mathbf{e}_i = \boldsymbol{T}(\boldsymbol{x})\mathbf{e}_i. \tag{3.6}$$

Hence, corresponding to the virtual displacements $\boldsymbol{v}(\boldsymbol{x})$ and rotations $\boldsymbol{w}(\boldsymbol{x})$ there exists a field

$$\mathbf{u} = (\boldsymbol{u},\boldsymbol{Q}) \tag{3.7}$$

composed of the displacement vector $\boldsymbol{u} \in E$ and the rotation tensor $\boldsymbol{Q} \in SO(3)$. It turns out that in regard to definitions (3.3) and (3.4) we have the following definitions of the stretching vector

$$\begin{aligned} \boldsymbol{\varepsilon}_\beta &\equiv \boldsymbol{y}_{,\beta} - \boldsymbol{t}_\beta \\ &= \boldsymbol{u}_{,\beta} + \boldsymbol{x}_{,\beta} - \boldsymbol{t}_\beta = \boldsymbol{u}_{,\beta} + \boldsymbol{t}_\beta^0 - \boldsymbol{t}_\beta = \boldsymbol{u}_{,\beta} + (\boldsymbol{1} - \boldsymbol{Q})\boldsymbol{t}_\beta^0 , \end{aligned} \tag{3.8}$$

and the bending vector

$$\boldsymbol{\kappa}_\beta \equiv \mathrm{ad}^{-1}(\boldsymbol{Q}_{,\beta}\boldsymbol{Q}^{\mathrm{T}}), \tag{3.9}$$

where map $\mathrm{ad}^{-1}(\ldots)$ is defined by (A.2).

Let us show that the virtual changes of (3.8) and (3.9) correspond to the virtual measures (3.3) and (3.4). A standard calculation of directional derivatives of (3.8) and (3.9) leads however to strain measures which are not objective in spatial representation. Therefore, we use the corotational derivative

$$\delta\boldsymbol{\varepsilon}_\beta \equiv \boldsymbol{Q}(\delta(\boldsymbol{Q}^T\boldsymbol{\varepsilon}_\beta)), \qquad \delta\boldsymbol{\kappa}_\beta \equiv \boldsymbol{Q}(\delta(\boldsymbol{Q}^T\boldsymbol{\kappa}_\beta)). \tag{3.10}$$

Now, for example, by making use of (A.8) we have

$$\begin{aligned} \delta\boldsymbol{\varepsilon}_\beta &\equiv \boldsymbol{Q}(\delta(\boldsymbol{Q}^T\boldsymbol{\varepsilon}_\beta)) = \boldsymbol{Q}(\delta\boldsymbol{Q}^T\boldsymbol{y}_{,\beta} + \boldsymbol{Q}^T\delta\boldsymbol{y}_{,\beta} - \delta\boldsymbol{Q}^T\boldsymbol{t}_\beta - \boldsymbol{Q}^T\delta\boldsymbol{t}_\beta) \\ &= -\mathrm{ad}\boldsymbol{w}\,\boldsymbol{y}_{,\beta} + \delta\boldsymbol{y}_{,\beta} + \mathrm{ad}\boldsymbol{w}\,\boldsymbol{t}_\beta - \delta\boldsymbol{t}_\beta = \\ &= \delta\boldsymbol{y}_{,\beta} - \mathrm{ad}\boldsymbol{w}\,\boldsymbol{y}_{,\beta} \\ &= \boldsymbol{v}_{,\beta} + \boldsymbol{y}_{,\beta} \times \boldsymbol{w} , \end{aligned} \tag{3.11}$$

i.e. the result exactly as in (3.3). Therefore, the strain measures (3.8) and (3.9) are natural in the sense that their corotational virtual changes result exactly from principle of virtual work. Both pairs of vectors $\delta\boldsymbol{\varepsilon}_\beta(\boldsymbol{x})$ and $\delta\boldsymbol{\kappa}_\beta(\boldsymbol{x})$ have three components each.

In the following FEM formulation the vector-matrix notation is introduced. Let us define the following energy conjugated objects:

$$\mathbf{w}=\begin{Bmatrix} v \\ w \end{Bmatrix}, \quad \mathbf{p}=\begin{Bmatrix} f \\ c \end{Bmatrix}, \quad \mathbf{s}^{*}=\begin{Bmatrix} n^{*} \\ m^{*} \end{Bmatrix}, \tag{3.12}$$

$$\tilde{\mathbf{e}}=\begin{Bmatrix} \varepsilon_{\beta} \\ \kappa_{\beta} \end{Bmatrix}=\begin{Bmatrix} \varepsilon_1 \\ \varepsilon_2 \\ \kappa_1 \\ \kappa_2 \end{Bmatrix}=\begin{Bmatrix} u_{,1}+(\mathbf{1}-\boldsymbol{Q})t_1^0 \\ u_{,2}+(\mathbf{1}-\boldsymbol{Q})t_2^0 \\ \mathrm{ad}^{-1}(\boldsymbol{Q}_{,1}\boldsymbol{Q}^{\mathrm{T}}) \\ \mathrm{ad}^{-1}(\boldsymbol{Q}_{,2}\boldsymbol{Q}^{\mathrm{T}}) \end{Bmatrix}, \quad \mathbf{s}=\begin{Bmatrix} n^{\beta} \\ m^{\beta} \end{Bmatrix}=\begin{Bmatrix} n^1 \\ n^2 \\ m^1 \\ m^2 \end{Bmatrix}. \tag{3.13}$$

The components of stress vector $\mathbf{s}$ are interpreted graphically in Fig 5. In $(3.13)_1$ by tilde we express the explicit dependence of strains on generalized displacements (3.7). With this notation, the virtual strain measures read

$$\delta\tilde{\mathbf{e}}=\begin{Bmatrix} \delta\varepsilon_1 \\ \delta\varepsilon_2 \\ \delta\kappa_1 \\ \delta\kappa_2 \end{Bmatrix}=\begin{Bmatrix} v_{,1}+(t_1+\varepsilon_1)\times w \\ v_{,2}+(t_2+\varepsilon_2)\times w \\ w_{,1} \\ w_{,2} \end{Bmatrix}. \tag{3.14}$$

We also define a vector corresponding to the surface deformation gradient

$$\delta\mathbf{d}=\begin{Bmatrix} v_{,1} \\ v_{,2} \\ w_{,1} \\ w_{,2} \\ w \end{Bmatrix}. \tag{3.15}$$

Therefore, in compact form we have

$$\delta\tilde{\mathbf{e}}(\mathbf{u})=\mathbf{B}(\mathbf{u})\,\mathbf{w}, \quad \delta\mathbf{d}=\mathbf{D}\,\mathbf{w}, \quad (\delta^2\tilde{\mathbf{e}}(\mathbf{u}))^T\,\mathbf{s}=\delta\mathbf{d}^T\mathbf{G}\delta\mathbf{d}, \tag{3.16}$$

where the following matrices (operators) are introduced

$$\mathbf{B}(\mathbf{u})=\begin{bmatrix} \mathbf{1}(.)_{,1} & (t_1+\varepsilon_1)\times(.) \\ \mathbf{1}(.)_{,2} & (t_2+\varepsilon_2)\times(.) \\ \mathbf{0} & \mathbf{1}(.)_{,1} \\ \mathbf{0} & \mathbf{1}(.)_{,2} \end{bmatrix}, \quad \mathbf{D}=\begin{bmatrix} \mathbf{1}(.)_{,1} & \mathbf{0} \\ \mathbf{1}(.)_{,2} & \mathbf{0} \\ \mathbf{0} & \mathbf{1}(.)_{,1} \\ \mathbf{0} & \mathbf{1}(.)_{,2} \\ \mathbf{0} & \mathbf{1} \end{bmatrix}, \tag{3.17}$$

$$\mathbf{G}(\mathbf{u}) = \begin{bmatrix} \mathbf{0} & \mathbf{0} & \mathbf{0} & \mathbf{0} & -\boldsymbol{n}^1\times(.) \\ \mathbf{0} & \mathbf{0} & \mathbf{0} & \mathbf{0} & -\boldsymbol{n}^2\times(.) \\ \mathbf{0} & \mathbf{0} & \mathbf{0} & \mathbf{0} & -\boldsymbol{m}^1\times(.) \\ \mathbf{0} & \mathbf{0} & \mathbf{0} & \mathbf{0} & -\boldsymbol{m}^2\times(.) \\ \boldsymbol{n}^1\times(.) & \boldsymbol{n}^2\times(.) & \mathbf{0} & \mathbf{0} & \mathbf{H} \end{bmatrix}, \tag{3.18}$$

with $\mathbf{H}(\mathbf{u}) = \boldsymbol{n}^\beta \otimes (\boldsymbol{t}_\beta + \boldsymbol{\varepsilon}_\beta) - (\boldsymbol{n}^\beta \cdot (\boldsymbol{t}_\beta + \boldsymbol{\varepsilon}_\beta))\mathbf{1}$.

If the field $\mathbf{u} = (\boldsymbol{u}, \boldsymbol{Q})$ satisfies the kinematical boundary conditions

$$U_A = \{\mathbf{u} \in U \mid \mathbf{u} = \mathbf{u}^* \quad \text{along} \quad \partial M_d\} \tag{3.19}$$

and the field $\mathbf{w} = (\boldsymbol{v}, \boldsymbol{w})$ satisfies the homogenous kinematical boundary conditions

$$W_A = \{\mathbf{w} \in W \mid \mathbf{w} = \mathbf{0} \quad \text{along} \quad \partial M_d\}, \tag{3.20}$$

then with the introduced notation the weak formulation (3.2) may be rewritten as the principle of virtual displacements

$$\begin{aligned} G[\mathbf{u};\mathbf{w}] &\equiv G_i[\mathbf{u};\mathbf{w}] - G_e[\mathbf{u};\mathbf{w}] = \\ &= \iint_M (\mathbf{B}(\mathbf{u})\,\mathbf{w})^T\, \tilde{\mathbf{s}}(\tilde{\mathbf{e}}(\mathbf{u}))\, da - \iint_M \mathbf{w}^T \mathbf{p}\, da - \int_{\partial M_f} \mathbf{w}^T \mathbf{s}^*\, dl \end{aligned} \tag{3.21}$$

with the constitutive relation given in the general form

$$\mathbf{s} = \mathbf{C}\mathbf{e}, \tag{3.22}$$

where $\mathbf{C}$ represents some constitutive matrix operator.

When linearized and approximated using FEM, the equation (3.21) leads to the displacement/rotation CAM finite elements (cf. [14]). The results obtained with the aid of these elements will serve as the reference here.

4. CONCEPT OF EAS FORMULATION

The EAS formulation is based on the assumption that the strain field may be expressed as the sum (cf. [19])

$$\mathbf{e} = \tilde{\mathbf{e}}(\mathbf{u}) + \hat{\mathbf{e}}\,, \tag{4.1}$$

where $\tilde{\mathbf{e}}(\mathbf{u})$ is the compatible strain defined by $(3.13)_1$ and $\hat{\mathbf{e}}$ is some independent enhancing part. Taking into account $(3.16)_1$ the virtual strains (4.1) may be written as

$$\delta\mathbf{e} = \delta\tilde{\mathbf{e}} + \delta\hat{\mathbf{e}} = \mathbf{B}(\mathbf{u})\mathbf{w} + \delta\hat{\mathbf{e}}\,. \tag{4.2}$$

Suppose now that there exists a strain energy function $\Phi(\mathbf{e}) = \Phi(\boldsymbol{\varepsilon}_\beta, \boldsymbol{\kappa}_\beta)$ chosen so, that when differentiated with respect to the strains it yields the constitutive relation (3.22), that is $\Phi(\mathbf{e})$ should be of the form

$$\Phi(\mathbf{e}) = \frac{1}{2}\mathbf{e}^T\mathbf{C}\mathbf{e}\,. \tag{4.3}$$

Assuming for convenience that there exists a potential, i.e. a functional $V[\mathbf{u};\mathbf{w}]$ such that $\delta V[\mathbf{u};\mathbf{w}] = -G_e[\mathbf{u};\mathbf{w}]$ we may derive, with the help of (4.1), the modified Hu-Washizu variational functional

$$\begin{aligned} W(\mathbf{u},\hat{\mathbf{e}},\hat{\mathbf{s}}) &= \iint_M \left(\Phi(\mathbf{e}) + \hat{\mathbf{s}}^T(\tilde{\mathbf{e}}(\mathbf{u}) - \hat{\mathbf{e}})\right) da + V(\mathbf{u}) \\ &= \iint_M \left(\Phi(\tilde{\mathbf{e}}(\mathbf{u}) + \hat{\mathbf{e}}) + \hat{\mathbf{s}}^T(-\hat{\mathbf{e}})\right) da + V(\mathbf{u})\,. \end{aligned} \tag{4.4}$$

The first variation of $(4.4)_2$ reads

$$\begin{aligned} \delta W[\mathbf{u},\hat{\mathbf{e}},\hat{\mathbf{s}};\mathbf{w},\delta\hat{\mathbf{e}},\delta\hat{\mathbf{s}}] = \\ \iint_M \left((\mathbf{B}\mathbf{w})^T\partial_{\mathbf{e}}\Phi + (\delta\hat{\mathbf{e}})^T(\partial_{\mathbf{e}}\Phi - \hat{\mathbf{s}}) - \delta\hat{\mathbf{s}}^T\hat{\mathbf{e}}\right) da \\ +\delta V[\mathbf{u};\mathbf{w}]\,. \end{aligned} \tag{4.5}$$

The solution of (4.5) satisfying $\delta W = 0$ is usually found numerically with the help of the Newton-type method and takes the form

$$\delta^2 W[\mathbf{u},\hat{\mathbf{e}},\hat{\mathbf{s}};\mathbf{w},\delta\hat{\mathbf{e}},\delta\hat{\mathbf{s}},\Delta\mathbf{u},\Delta\hat{\mathbf{e}},\Delta\hat{\mathbf{s}}] + \delta W[\mathbf{u},\hat{\mathbf{e}},\hat{\mathbf{s}};\mathbf{w},\delta\hat{\mathbf{e}},\delta\hat{\mathbf{s}}] = 0\,. \tag{4.6}$$

Equation (4.6) requires linearization. i.e. computing of directional derivative of the respective functional which leads to

$$\begin{aligned}
&\iint_M \Big((\Delta\delta\tilde{\mathbf{e}}(\mathbf{u}))^T \partial_{\mathbf{e}}\Phi + (\delta\tilde{\mathbf{e}}(\mathbf{u}))^T \partial^2_{\mathbf{ee}}\Phi \Delta\tilde{\mathbf{e}}(\mathbf{u}) + \\
&\quad (\delta\hat{\mathbf{e}})^T \partial^2_{\mathbf{ee}}\Phi \Delta\tilde{\mathbf{e}}(\mathbf{u}) + (\delta\tilde{\mathbf{e}}(\mathbf{u}))^T \partial^2_{\mathbf{ee}}\Phi \Delta\hat{\mathbf{e}} + \\
&\quad (\delta\hat{\mathbf{e}})^T \partial^2_{\mathbf{ee}}\Phi \Delta\hat{\mathbf{e}} - \underline{\delta\hat{\mathbf{s}}^T \Delta\hat{\mathbf{e}}} - \underline{(\delta\hat{\mathbf{e}})^T \Delta\hat{\mathbf{s}}} \Big) da + \\
&\quad \delta^2 V[\mathbf{u};\mathbf{w},\Delta\mathbf{u}] + \\
&\iint_M \Big((\mathbf{B}\mathbf{w})^T \partial_{\mathbf{e}}\Phi + \delta\hat{\mathbf{e}}^T \partial_{\mathbf{e}}\Phi - \underline{\delta\hat{\mathbf{e}}^T \hat{\mathbf{s}}} - \underline{\delta\hat{\mathbf{s}}^T \hat{\mathbf{e}}} \Big) da + \\
&\quad \delta V[\mathbf{u};\mathbf{w}] = 0 .
\end{aligned} \tag{4.7}$$

We now invoke some important facts concerning the EAS elements. To ensure the stability of the enhanced strain approximation and to satisfy the patch-test, it is required (cf. [19]) that the so-called orthogonality conditions should hold

$$\iint_M \delta\hat{\mathbf{s}}^T \hat{\mathbf{e}} da = 0 , \quad \iint_M \delta\hat{\mathbf{e}}^T \hat{\mathbf{s}} da = 0 . \tag{4.8}$$

Consequently, the underlined terms involving variations of the strains and stresses drop out from (4.7). With the relations

$$\partial^2_{\mathbf{ee}}\Phi = \mathbf{C} , \quad \partial_{\mathbf{e}}\Phi = \mathbf{s}(\mathbf{e}) = \mathbf{C}(\tilde{\mathbf{e}}(\mathbf{u}) + \hat{\mathbf{e}}) \tag{4.9}$$

the three-field functional (4.4) reduces to the two-field functional with $(\mathbf{u}, \hat{\mathbf{e}})$ as the independent variables. Therefore, from (4.5) we have

$$\begin{aligned}
&\delta W[\mathbf{u},\hat{\mathbf{e}};\mathbf{w},\delta\hat{\mathbf{e}}] = \\
&\qquad \iint_M \left(\mathbf{B}\mathbf{w} + \delta\hat{\mathbf{e}}^T \right)^T \mathbf{s}(\mathbf{e}) da + \delta V[\mathbf{u};\mathbf{w}] .
\end{aligned} \tag{4.10}$$

In the sequel, due to the main goal of the paper, we confine our attention to dead loads, thereby $\delta^2 V[\mathbf{u};\mathbf{w},\Delta\mathbf{u}] = 0$ and from (4.6) and $(3.16)_3$ we have

$$\begin{aligned}
&\delta^2 W[\mathbf{u},\hat{\mathbf{e}};\mathbf{w},\delta\hat{\mathbf{e}},\Delta\mathbf{u},\Delta\hat{\mathbf{e}}] + \delta W[\mathbf{u},\hat{\mathbf{e}};\mathbf{w},\delta\hat{\mathbf{e}}] \equiv \\
&\quad \iint_M \Big((\delta\mathbf{d}^T \mathbf{G} \delta\mathbf{d} + (\delta\tilde{\mathbf{e}}(\mathbf{u}))^T \mathbf{C} \Delta\tilde{\mathbf{e}}(\mathrm{u}) + \\
&\quad (\delta\hat{\mathbf{e}})^T \mathbf{C} \Delta\tilde{\mathbf{e}}(\mathrm{u}) + (\delta\tilde{\mathbf{e}}(\mathbf{u}))^T \mathbf{C} \Delta\hat{\mathbf{e}} + (\delta\hat{\mathbf{e}})^T \mathbf{C} \Delta\hat{\mathbf{e}} \Big) da \\
&\quad \iint_M \Big((\mathbf{B}\mathbf{w})^T \mathbf{s} + \delta\hat{\mathbf{e}}^T \mathbf{s} \Big) da + \delta V[\mathbf{u};\mathbf{w}] = 0 .
\end{aligned} \tag{4.11}$$

The above equation forms the foundation of the proposed EAS element.

5. FEM DISCRETIZATION

5.1. INTERPOLATION

From the above development it is seen that we have four main types of variables belonging to: the vector space E, the rotation group $SO(3)$, and the space of skew-symmetric tensors $so(3)$. In addition, we have the enhanced strain variables. Each type of the variables undergoes different way of interpolation. Below, we remind the interpolation schemes for each type of the variables.

5.1.1. INTERPOLATION OF VECTOR VARIABLES

Following the standard FEM approach, we approximate the base surface of the shell as a sum

$$M \approx M_h = \sum_{e=1}^{N_e} \Pi_{(e)} , \tag{5.1}$$

where N_e is the number of finite elements. A typical finite element $\Pi_{(e)}$ is defined as a smooth image of the so-called standard element $\pi_{(e)}$. Here $\pi_{(e)} = [-1,+1]\times[-1,+1]$ is the element in the parent (natural) domain $\boldsymbol{\xi} = (\xi_1, \xi_2)$. Within each 4-node element the vector-type variables $\boldsymbol{x}$, $\boldsymbol{y}$ and $\boldsymbol{v}$ are interpolated using the Lagrange polynomials

$$\boldsymbol{x}(\boldsymbol{\xi}) = \sum_{a=1}^{4} L_a(\boldsymbol{\xi})\, \boldsymbol{x}_a , \tag{5.2}$$

where

$$\begin{aligned} L_1(\boldsymbol{\xi}) &= \frac{1}{4}(1+\xi_1)(1+\xi_2), \quad L_2(\boldsymbol{\xi}) = \frac{1}{4}(1-\xi_1)(1+\xi_2) , \\ L_3(\boldsymbol{\xi}) &= \frac{1}{4}(1-\xi_1)(1-\xi_2), \quad L_4(\boldsymbol{\xi}) = \frac{1}{4}(1+\xi_1)(1-\xi_2) \end{aligned} \tag{5.3}$$

are the standard shape functions of bilinear quadrilateral element.

In our approach, every node of FEM mesh in the reference configuration is defined by the position vector $\boldsymbol{x}_a$ and the rotation tensor $(\boldsymbol{T}_0)_a$. Both $\boldsymbol{x}_a$ and tensor $(\boldsymbol{T}_0)_a$ are treated here as independent input data.

Since definitions of the strain measures require the derivatives with respect to the arc-length parameters $\{s_\beta\}$, we have to calculate such derivatives. In view of $(2.6)_1$ from the chain rule we have

$$\boldsymbol{t}_\beta^0(\boldsymbol{\xi}) = \frac{\partial \boldsymbol{x}(\boldsymbol{\xi})}{\partial s_\beta} = \frac{\partial \boldsymbol{x}(\boldsymbol{\xi})}{\partial \xi_\alpha}\frac{\partial \xi_\alpha}{\partial s_\beta}. \tag{5.4}$$

However, we also have $\boldsymbol{t}_i^0(\boldsymbol{\xi}) = \boldsymbol{T}_0(\boldsymbol{\xi})\mathbf{e}_i$ so by forming the scalar product we arrive at

$$\boldsymbol{t}_\alpha^0(\boldsymbol{\xi})\cdot\boldsymbol{t}_\beta^0(\boldsymbol{\xi}) = \frac{\partial \xi_\lambda}{\partial s_\alpha}\frac{\partial \boldsymbol{x}(\boldsymbol{\xi})}{\partial \xi_\lambda}\cdot\boldsymbol{t}_\beta^0(\boldsymbol{\xi}) = \frac{\partial \xi_\lambda}{\partial s_\alpha}\frac{\partial \boldsymbol{x}(\boldsymbol{\xi})}{\partial \xi_\lambda}\cdot\boldsymbol{T}_0(\boldsymbol{\xi})\,\mathbf{e}_\beta = \delta_{\alpha\beta}. \tag{5.5}$$

In the matrix form, for two vectors of the surface base we have

$$\begin{bmatrix} \xi_{1,1} & \xi_{2,1} \\ \xi_{1,2} & \xi_{2,2} \end{bmatrix}\begin{bmatrix} (\partial \boldsymbol{x}/\partial\xi_1)\cdot\boldsymbol{t}_1^0 & (\partial \boldsymbol{x}/\partial\xi_1)\cdot\boldsymbol{t}_2^0 \\ (\partial \boldsymbol{x}/\partial\xi_2)\cdot\boldsymbol{t}_1^0 & (\partial \boldsymbol{x}/\partial\xi_2)\cdot\boldsymbol{t}_2^0 \end{bmatrix} = \begin{bmatrix} 1 & 0 \\ 0 & 1 \end{bmatrix}. \tag{5.6}$$

Since the terms

$$s_{\alpha,\beta} = (\partial \boldsymbol{x}/\partial\xi_\beta)\cdot\boldsymbol{t}_\alpha^0 \tag{5.7}$$

follow from the initial geometry through (5.2), the solution of (5.6) with respect to $[\xi_{\beta,\lambda}]$ does not create a problem. Now, the derivatives of the shape functions with respect to $\{s_\beta\}$ are given by

$$(L_a),_\beta = \frac{\partial L_\alpha(\boldsymbol{\xi})}{\partial s_\beta} = \frac{\partial L_\alpha(\boldsymbol{\xi})}{\partial \xi_1}\xi_{1,\beta} + \frac{\partial L_\alpha(\boldsymbol{\xi})}{\partial \xi_2}\xi_{2,\beta} \tag{5.8}$$

and the area element is transformed using

$$da = ds_1 ds_2 = \alpha(\boldsymbol{\xi})\,d\xi_1 d\xi_2, \tag{5.9}$$

where

$$\alpha(\boldsymbol{\xi}) = \det\begin{bmatrix} (\partial \boldsymbol{x} / \partial \xi_1)\cdot \boldsymbol{t}_1^0 & (\partial \boldsymbol{x} / \partial \xi_1)\cdot \boldsymbol{t}_2^0 \\ (\partial \boldsymbol{x} / \partial \xi_2)\cdot \boldsymbol{t}_1^0 & (\partial \boldsymbol{x} / \partial \xi_2)\cdot \boldsymbol{t}_2^0 \end{bmatrix}. \tag{5.10}$$

5.1.2. INTERPOLATION ON SO(3) GROUP

The interpolation of elements from $SO(3)$ group is more complex. This is due to the fact that relation (5.2), when applied to objects from $SO(3)$, takes the object out of this group. Therefore such interpolation can not be applied directly here and additional steps are required to ensure that an interpolated object belonging to the rotation group would always remain in that group after interpolation. Such schemes have been already proposed. Reference [14] provides the straightforward approach, while in [15] (see also [32]) the details of the more precise procedure are given. This is completely general procedure applicable to any manifold. In particular, it may be specified for arbitrary parametrization of the rotation group. The approach first presented in [15] practically removes the singularity of parametrization within a finite element due to some transport-type operation to the neighborhood of the neutral element $\mathbf{1} \in SO(3)$. Here, we particularize the procedure for the canonical parametrization of $\boldsymbol{Q}$ and $\boldsymbol{Q}_{,\beta}$ (see (3.9)) used in this paper.

1) At each element, from the discrete nodal set $\boldsymbol{Q}_a = \boldsymbol{Q}(\boldsymbol{\xi}_a)$, $a = 1,2,3,4$, of function $\boldsymbol{Q}(\boldsymbol{\xi})$ $(\boldsymbol{\xi} \in \pi_{(e)})$, we select some representative tensor $\bar{\boldsymbol{Q}} \in SO(3)$. In this work, we assume that the best representative from four nodal tensors is that found as a result of orthonormalization of the mean values (over element nodes) of the components of vectors t_{ij}^a, $\boldsymbol{t}_j^a = t_{ij}^a \mathbf{e}_i \Rightarrow \mathbf{t}_j^a$ from the set $\boldsymbol{Q}_a \Rightarrow \mathbf{Q}_a \equiv [\mathbf{t}_1^a \,|\, \mathbf{t}_2^a \,|\, \mathbf{t}^a \equiv \mathbf{t}_3^a]$. The normal vector $\boldsymbol{t}_3^a \Rightarrow \mathbf{t}_3^a$ is always distinguished.

2) With the help of $\bar{\boldsymbol{Q}} \in SO(3)$ we transform the nodal element tensors to the neighborhood of the neutral element of the group $\mathbf{1} \in SO(3)$ (where in the canonical parametrization the error of interpolation is the smallest) by computing at each node a tensor

$$\boldsymbol{R}_a = \bar{\boldsymbol{Q}}^T \boldsymbol{Q}_a , \qquad \bar{\boldsymbol{Q}} = const . \tag{5.11}$$

3) Since the tensors $\boldsymbol{R}_a$ belong to the neighborhood of $\mathbf{1} \in SO(3)$, at each node we compute in a nonsingular manner the components of the axial vectors $\boldsymbol{\varphi}_a$ by making use of (A.6) and (A.7), i.e.

$$\varphi_a = \operatorname{acos}\left(\frac{1}{2}(tr\boldsymbol{R}_a - 1)\right), \quad \boldsymbol{\varphi}_a = \frac{1}{2\sin\varphi_a}\operatorname{ad}^{-1}(\boldsymbol{R}_a - \boldsymbol{R}_a^{\,T}) . \tag{5.12}$$

4) We interpolate $\tilde{\boldsymbol{\varphi}}(\boldsymbol{\xi})$ as elements of R^3 using

$$\tilde{\boldsymbol{\varphi}}(\boldsymbol{\xi}) \to \begin{Bmatrix} \tilde{\varphi}_1(\boldsymbol{\xi}) \\ \tilde{\varphi}_2(\boldsymbol{\xi}) \\ \tilde{\varphi}_3(\boldsymbol{\xi}) \end{Bmatrix} = \sum_{a=1}^{4} L_a(\boldsymbol{\xi}) \begin{Bmatrix} \varphi_{1a} \\ \varphi_{2a} \\ \varphi_{3a} \end{Bmatrix} = \sum_{a=1}^{4} L_a(\boldsymbol{\xi})\boldsymbol{\varphi}_a , \tag{5.13}$$

and derivatives $\boldsymbol{\varphi}_{,\beta}$ according to

$$\tilde{\boldsymbol{\varphi}}(\boldsymbol{\xi})_{,\beta} \to \begin{Bmatrix} \tilde{\varphi}_1(\boldsymbol{\xi})_{,\beta} \\ \tilde{\varphi}_2(\boldsymbol{\xi})_{,\beta} \\ \tilde{\varphi}_3(\boldsymbol{\xi})_{,\beta} \end{Bmatrix} = \sum_{a=1}^{4} L_a(\boldsymbol{\xi})_{,\beta} \begin{Bmatrix} \varphi_{1a} \\ \varphi_{2a} \\ \varphi_{3a} \end{Bmatrix} = \sum_{a=1}^{4} L_a(\boldsymbol{\xi})_{,\beta}\boldsymbol{\varphi}_a , \tag{5.14}$$

where derivatives $L_a(\boldsymbol{\xi})_{,\beta}$ are given by (5.8).

5) We compute the tensors $\tilde{\boldsymbol{R}}(\xi)$ and $\tilde{\boldsymbol{R}}(\xi),_{\beta}$ by using $\tilde{\boldsymbol{\varphi}}(\xi)$ and $\tilde{\boldsymbol{\varphi}}(\xi),_{\beta}$ according to

$$\tilde{\boldsymbol{R}}(\xi) = \mathbf{1} + \tilde{a}(\xi)\tilde{\boldsymbol{\Phi}}(\xi) + \tilde{b}(\xi)\left(\tilde{\boldsymbol{\Phi}}(\xi)\right)^2, \tag{5.15}$$

$$\begin{aligned}\tilde{\boldsymbol{R}}(\xi),_{\beta} = \tilde{a}(\xi),_{\beta}\,\tilde{\boldsymbol{\Phi}}(\xi) + \tilde{a}(\xi)\tilde{\boldsymbol{\Phi}}(\xi),_{\beta} + \\ + \tilde{b}(\xi),_{\beta}\left(\tilde{\boldsymbol{\Phi}}(\xi)\right)^2 + \tilde{b}(\xi)\left(\tilde{\boldsymbol{\Phi}}(\xi),_{\beta}\,\tilde{\boldsymbol{\Phi}}(\xi) + \tilde{\boldsymbol{\Phi}}(\xi)\tilde{\boldsymbol{\Phi}}(\xi),_{\beta}\right),\end{aligned} \tag{5.16}$$

where

$$\tilde{\boldsymbol{\Phi}}(\xi) = \mathrm{ad}(\tilde{\boldsymbol{\varphi}}(\xi)), \quad \tilde{\boldsymbol{\Phi}}(\xi),_{\beta} = \mathrm{ad}(\tilde{\boldsymbol{\varphi}}(\xi),_{\beta}), \quad \tilde{\varphi}(\xi) = \left\|\tilde{\boldsymbol{\varphi}}(\xi)\right\| \tag{5.17}$$

$$\tilde{a}(\xi) = \frac{\sin\tilde{\varphi}(\xi)}{\tilde{\varphi}(\xi)}, \quad \tilde{b}(\xi) = \frac{1-\cos\tilde{\varphi}(\xi)}{\tilde{\varphi}(\xi)}, \tag{5.18}$$

$$\tilde{a}(\xi),_{\beta} = \frac{\cos\tilde{\varphi}(\xi) - \tilde{a}(\xi)}{\tilde{\varphi}(\xi)^2}\tilde{\boldsymbol{\varphi}}(\xi)\cdot\tilde{\boldsymbol{\varphi}}(\xi),_{\beta}, \quad \tilde{b}(\xi),_{\beta} = \frac{-2\tilde{b}(\xi) - \tilde{a}(\xi)}{\tilde{\varphi}(\xi)^2}\tilde{\boldsymbol{\varphi}}(\xi)\cdot\tilde{\boldsymbol{\varphi}}(\xi),_{\beta}. \tag{5.19}$$

6) W compute interpolated tensors $\tilde{\boldsymbol{Q}}(\xi)$ and $\tilde{\boldsymbol{Q}},_{\beta}(\xi)$ by using $\tilde{\boldsymbol{R}}(\xi)$ and $\tilde{\boldsymbol{R}}(\xi),_{\beta}$

$$\tilde{\boldsymbol{Q}}(\xi) = \bar{\boldsymbol{Q}}\tilde{\boldsymbol{R}}(\xi), \quad \bar{\boldsymbol{Q}} = const, \tag{5.20}$$

$$\tilde{\boldsymbol{Q}},_{\beta}(\xi) = \bar{\boldsymbol{Q}}\tilde{\boldsymbol{R}}(\xi),_{\beta}. \tag{5.21}$$

The tensor $\boldsymbol{Q}$ discussed above represents not only the rotation tensor of shell deformation but also other proper orthogonal tensors such as $\boldsymbol{T}_0$, $\boldsymbol{T}$. However, for each of these objects, a proper representative corresponding to $\bar{\boldsymbol{Q}}$ must be selected individually at each element.

5.1.3. INTERPOLATION ON so(3) GROUP

The vector of virtual rotations $\boldsymbol{w} \in so(3)$ is interpolated after transformation to the fixed frame $\mathbf{e}_i$, i.e.

$$\boldsymbol{w}(\boldsymbol{\xi}) = w_i(\boldsymbol{\xi})\,\boldsymbol{t}_i(\boldsymbol{\xi}) = \overline{w}_j(\boldsymbol{\xi})\,\mathbf{e}_j = \overline{w}_j(\boldsymbol{\xi})\,\boldsymbol{T}^T(\boldsymbol{\xi})\,\boldsymbol{t}_j(\boldsymbol{\xi})\,, \tag{5.22}$$

which yields the following interpolating scheme

$$\begin{Bmatrix} \tilde{w}_1(\boldsymbol{\xi}) \\ \tilde{w}_2(\boldsymbol{\xi}) \\ \tilde{w}_3(\boldsymbol{\xi}) \end{Bmatrix} = \mathbf{T}(\boldsymbol{\xi}) \sum_{a=1}^{N} L_a(\boldsymbol{\xi}) \begin{Bmatrix} \overline{w}_{1a} \\ \overline{w}_{1a} \\ \overline{w}_{1a} \end{Bmatrix}, \qquad \boldsymbol{\xi} \in \pi_{(e)}\,. \tag{5.23}$$

In this way, one can easily describe the junctions of different shell branches. Of course, to evaluate the derivatives in (5.23) one requires to interpolate $\mathbf{T}(\boldsymbol{\xi})$ according to the schemes described above.

5.1.4. INTERPOLATION OF EAS VARIABLES

In EAS approach, the vector of enhancing strains (4.1) and its variations (4.2) or increments, with the components in the base $\{\boldsymbol{t}_i, i = 1,2,3\}$, are interpolated within typical element according to

$$\hat{\mathbf{e}}(\boldsymbol{\xi}) = \mathbf{P}(\boldsymbol{\xi})\boldsymbol{\beta}_{(e)}\,, \qquad \Delta\hat{\mathbf{e}}(\boldsymbol{\xi}) = \mathbf{P}(\boldsymbol{\xi})\Delta\boldsymbol{\beta}_{(e)}\,, \tag{5.24}$$

where $\boldsymbol{\beta}_{(e)}$ and $\Delta\boldsymbol{\beta}_{(e)}$ are the vectors collecting the enhancing strain parameters on the level of the parent element in $\boldsymbol{\xi} = (\xi_1, \xi_2)$ coordinates. Matrix $\mathbf{P}(\boldsymbol{\xi})$ has the following form (cf. [19])

$$\mathbf{P}(\boldsymbol{\xi}) = \frac{\alpha_0}{\alpha(\boldsymbol{\xi})}\mathbf{M}^{-T}(\boldsymbol{\xi})\Big|_{\boldsymbol{\xi}=\mathbf{0}}\mathbf{H}(\boldsymbol{\xi})\,. \tag{5.25}$$

The transformation matrix $\mathbf{M}$ from (5.25) is built based on the "push–forward" operation known from tensor calculus. It maps the polynomial shape functions $\mathbf{H}$ defined in $\boldsymbol{\xi} = (\xi_1, \xi_2)$ domain into $\{s_\beta\}$ domain. In order to satisfy the patch-test in the sense given in [21], the transformation is confined to the origin of an element $\boldsymbol{\xi} = (0,0)$ so that the components of $\mathbf{M}$ are constant. In (5.25), α_0 denotes the value of determinant

(5.10) evaluated at the element origin. The size of $\mathbf{M}$ is determined by the type of problem and the number of components of the strain vector that are to be enhanced.

In reference [2], it was argued that application of EAS method to bending part of the strain has negligible influence on the accuracy of FEM calculations and makes the calculations more time-consuming. The same fact was concluded in [15] and [16] in the context of mixed formulation yielding the semi-mixed elements, developed on the grounds of the same theory of shell as used here. Therefore, in this paper only stretching and shear strains defined by $(3.13)_1$

$$\mathbf{e_e} = \{\varepsilon_{11}\ \varepsilon_{22}\ \varepsilon_{12}\ \varepsilon_{21}\ \varepsilon_1\ \varepsilon_2\}^T \tag{5.26}$$

are subjected to EAS technique. The bending component of strain vector $(3.13)_1$ is not enhanced. Therefore, analogously to the semi-mixed formulation of [15] and [16], we propose a notion "semi-enhanced element". As it may be observed, due to the presence of curvatures and drilling couples, the membrane strains are not symmetric in the third and the fourth slot of (5.26) in contrast to the majority of papers concerned with application of EAS method. In addition, in comparison with the original formulation [19], (5.26) contains also components associated with shear. This fact requires special attention in the forthcoming selection of enhancing strains.

According to the order of components assumed in (5.26), the matrix $\mathbf{M}$ takes the form

$$\underset{6\times 6}{\mathbf{M}} = \begin{bmatrix} s_{1,1}\,s_{1,1} & s_{1,2}\,s_{1,2} & s_{1,2}\,s_{1,1} & s_{1,1}\,s_{1,2} & 0 & 0 \\ s_{2,1}\,s_{2,1} & s_{2,2}\,s_{2,2} & s_{2,2}\,s_{2,1} & s_{2,1}\,s_{2,2} & 0 & 0 \\ s_{1,1}\,s_{2,1} & s_{1,2}\,s_{2,2} & s_{1,1}\,s_{2,2} & s_{1,2}\,s_{2,1} & 0 & 0 \\ s_{1,1}\,s_{2,1} & s_{1,2}\,s_{2,2} & s_{1,2}\,s_{2,1} & s_{1,1}\,s_{2,2} & 0 & 0 \\ 0 & 0 & 0 & 0 & s_{1,1} & s_{1,2} \\ 0 & 0 & 0 & 0 & s_{2,1} & s_{2,2} \end{bmatrix}, \tag{5.27}$$

where the elements $s_{\alpha,\beta}$ are computed from (5.7). As in any approximating method, the crucial point of defining EAS element is the matrix $\mathbf{H}(\boldsymbol{\xi})$ in (5.25). In order to pass the patch-test, as a consequence of (4.8) (see [19] for details), this matrix should satisfy the condition

$$\int_{\pi_{(e)}} \mathbf{H}(\boldsymbol{\xi}) d\boldsymbol{\xi} = \mathbf{0}. \tag{5.28}$$

The appropriate choice of $\mathbf{H}$ determines the properties of the EAS elements. As to selection of the enhancing strain field some clues may be found in the following (but not limited to) papers: [2], [3], [4], [19], [23], [24]. For example, in [2] two finite elements were proposed: EAS4-ANS and EAS7-ANS with four and seven parameters used respectively to enhance the symmetric membrane strains. In contrast to [3], [4] and this paper, to deal with the shear locking the authors used the ANS concept from [18]. Other authors, like for example [3], [4], [24], successfully tried to use the EAS concept to all components of the strain vector. Yet, as it has been already pointed out, the results from the literature are for symmetric membrane strains and, as such, are to be applied here with caution.

The proper selection and verification of various enhancing fields was the topics of extensive studies in Ph.D. thesis of the second author. By modifying and combining the enhancing fields known form the literature, four elements were proposed. By solving a number of examples, one element denoted EAS(14)m1 was selected and it is presented in this paper. In this element fourteen parameters are used to enhance strain field.

The membrane strains ε_{11} and ε_{22} are enhanced as in the element EAS7-ANS from [2]. To enhance the shear strains ε_1 and ε_2 we follow the concept from [3], which is based on the derivatives of the bubble function

$$N = \left(1-(\xi_1)^2\right)\left(1-(\xi_2)^2\right). \tag{5.29}$$

Finally, for the membrane strains ε_{12} and ε_{21} our own enhancing fields are proposed, extending the concept from [2] and [3]. The explicit form of the matrix H for EAS(14)m1 element is

$$\underset{6\times 14}{\mathbf{H}(\boldsymbol{\xi})} = \begin{bmatrix} \xi^1 & \xi^1\xi^2 & & & & & & & & & & & & \\ & & \xi^2 & \xi^1\xi^2 & & & & & & & & & & \\ & & & & \xi^1 & \xi^1\xi^2 & & & & & & & & \\ & & & & & & \xi^2 & \xi^1\xi^2 & & & & & & \\ & & 0 & & & & & & a & b & ab & & & \\ & & & & & & & & & & & b & a & ab \end{bmatrix}. \tag{5.30}$$

Here $a = 2\xi_1((\xi_2)^2-1)$, $b = 2\xi_2((\xi_1)^2-1)$ are just derivatives of the bubble function (5.29).

5.2. ELEMENT MATRICES

At each node of the finite element there are six nodal dofs: three virtual (incremental) translations and three virtual (incremental) parameters of rotations referred to the global frame $\{\mathbf{e}_i\}$. These dofs compose the nodal displacement vector and element displacement vector, respectively, as given below

$$\delta\boldsymbol{q}_a = \begin{Bmatrix} \boldsymbol{v}_a \\ \overline{\boldsymbol{w}}_a \end{Bmatrix} = \begin{Bmatrix} v_1 \\ v_2 \\ v_3 \\ \overline{w}_1 \\ \overline{w}_2 \\ \overline{w}_3 \end{Bmatrix}, \qquad \delta\mathbf{q}_{(e)} = \begin{Bmatrix} \delta\boldsymbol{q}_1 \\ \delta\boldsymbol{q}_2 \\ \delta\boldsymbol{q}_3 \\ \delta\boldsymbol{q}_4 \end{Bmatrix}. \tag{5.31}$$

From the shape functions (5.3) we form the matrix

$$\overline{\mathsf{L}}_a(\boldsymbol{\xi}) = \begin{bmatrix} L_a(\boldsymbol{\xi})\mathbf{1} & \mathbf{0} \\ \mathbf{0} & L_a(\boldsymbol{\xi})\mathbf{1} \end{bmatrix}, \qquad \overline{\mathsf{L}}(\boldsymbol{\xi}) = [\,\overline{\mathsf{L}}_1(\boldsymbol{\xi})\ \overline{\mathsf{L}}_2(\boldsymbol{\xi})\ \overline{\mathsf{L}}_3(\boldsymbol{\xi})\ \overline{\mathsf{L}}_4(\boldsymbol{\xi})\,], \tag{5.32}$$

Hence, for a single element the following interpolation scheme holds

$$\mathbf{w}(\xi)=\begin{Bmatrix} v(\xi) \\ \bar{w}(\xi) \end{Bmatrix}=\bar{\mathbf{L}}(\xi)\,\delta\mathbf{q}_{(e)}\,. \tag{5.33}$$

However, in the light of interpolating scheme for the vector of virtual rotations (5.22) one arrives at

$$\mathbf{w}(\xi)=\mathbf{L}(\xi)\,\delta\mathbf{q}_{(e)}\,,\qquad \mathbf{L}(\xi)=\bar{\mathbf{Y}}(\xi)\bar{\mathbf{L}}(\xi)\,,\qquad \bar{\mathbf{Y}}(\xi)=\begin{bmatrix} \mathbf{1} & \mathbf{0} \\ \mathbf{0} & \mathbf{T}^{T}(\xi) \end{bmatrix}. \tag{5.34}$$

Equations $(5.34)_1$ are also used for incremental displacements and rotations

$$\Delta\mathbf{u}(\xi)=\mathbf{L}(\xi)\,\Delta\mathbf{q}_{(e)}\,. \tag{5.35}$$

Since only the stretching and shear strains are enhanced, the following decompositions of the strain vector (3.13), the strain-displacement matrix $(5.40)_1$ and the internal force vector $(3.13)_2$ are introduced:

$$\mathbf{e}=\begin{Bmatrix} \tilde{\mathbf{e}}_{\mathbf{e}} \\ \tilde{\mathbf{e}}_{\mathbf{k}} \end{Bmatrix}+\begin{Bmatrix} \hat{\mathbf{e}}_{\mathbf{e}} \\ \mathbf{0} \end{Bmatrix},\qquad \mathbf{B}=\begin{Bmatrix} \mathbf{B}_{\mathbf{e}} \\ \mathbf{B}_{\mathbf{k}} \end{Bmatrix},\qquad \mathbf{s}=\begin{Bmatrix} \mathbf{s}_{\mathbf{e}} \\ \mathbf{s}_{\mathbf{k}} \end{Bmatrix}. \tag{5.36}$$

By substituting (5.33), (5.35) and $(5.24)_2$ to (4.5) and (4.11) we arrive at

$$\begin{aligned} (\mathbf{K}_G^{(e)}+\mathbf{K}_M^{(e)})\,\Delta\mathbf{q}_{(e)}+(\mathbf{K}_{\beta\mathbf{q}}^{(e)})^{T}\,\Delta\boldsymbol{\beta}_{(e)} &= \mathbf{p}^{(e)}-\mathbf{r}_d^{(e)}, \\ \mathbf{K}_{\beta\mathbf{q}}^{(e)}\,\Delta\mathbf{q}_{(e)}+\mathbf{K}_{\beta\beta}^{(e)}\,\Delta\boldsymbol{\beta}_{(e)} &= -\mathbf{r}_{\beta}^{(e)}\,, \end{aligned} \tag{5.37}$$

where we have defined the following matrices:

$$\mathbf{K}_M^{(e)}=\iint_{\Pi_{(e)}}\bar{\mathbf{B}}^{T}\mathbf{C}\bar{\mathbf{B}}\,da\,,\qquad \mathbf{K}_G^{(e)}=\iint_{\Pi_{(e)}}\bar{\mathbf{D}}^{T}\mathbf{G}\bar{\mathbf{D}}\,da\,, \tag{5.38}$$

$$\mathbf{K}_{\beta\beta}^{(e)}=\iint_{\Pi_{(e)}}\mathbf{P}^{T}\mathbf{C}\mathbf{P}da\,,\qquad \mathbf{K}_{\beta\mathbf{q}}^{(e)}=\iint_{\Pi_{(e)}}\mathbf{P}^{T}\mathbf{C}\bar{\mathbf{B}}_{\mathbf{e}}da\,, \tag{5.39}$$

$$\bar{\mathbf{B}}=\mathbf{B}\mathbf{L}\,,\qquad \bar{\mathbf{D}}=\mathbf{D}\mathbf{L}\,, \tag{5.40}$$

$$\mathbf{r}_d^{(e)}=\iint_{\Pi_{(e)}}\bar{\mathbf{B}}^{T}\mathbf{s}(\mathbf{u})\,da\,,\qquad \mathbf{r}_{\beta}^{(e)}=\iint_{\Pi_{(e)}}\mathbf{P}^{T}\mathbf{s}_{\mathbf{e}}\,da\,, \tag{5.41}$$

$$\mathbf{p}^{(e)} = \iint_{\Pi_{(e)}} \mathbf{L}^T \mathbf{p}(q)\, da\,. \tag{5.42}$$

Since the enhancing fields require only piece-wise continuity (cf. [19]), analogously as the fields of generalized stresses in the semi-mixed formulation (cf.[15], [16]), they are eliminated on the element level by static condensation

$$\Delta\boldsymbol{\beta}_{(e)} = -(\mathbf{K}_{\boldsymbol{\beta}\boldsymbol{\beta}}^{(e)})^{-1}(\mathbf{K}_{\boldsymbol{\beta}\mathbf{q}}^{(e)}\Delta\mathbf{q}_{(e)} + \mathbf{r}_{\boldsymbol{\beta}}^{(e)})\,, \tag{5.43}$$

which yields the classical form of the linearized equation for a typical element

$$\mathbf{K}_T^{(e)}\Delta\mathbf{q}_{(e)} = \Delta\mathbf{p}^{(e)} + \mathbf{j}^{(e)}\,, \qquad \mathbf{j}^{(e)} = \mathbf{p}^{(e)} - \mathbf{r}^{(e)}\,, \tag{5.44}$$

where the tangent stiffness matrix and the element residual vector (for dead loads) have the forms typical for mixed-type elements

$$\mathbf{K}_T^{(e)} = \mathbf{K}_G^{(e)} + \mathbf{K}_M^{(e)} - (\mathbf{K}_{\boldsymbol{\beta}\mathbf{q}}^{(e)})^T(\mathbf{K}_{\boldsymbol{\beta}\boldsymbol{\beta}}^{(e)})^{-1}\mathbf{K}_{\boldsymbol{\beta}\mathbf{q}}^{(e)}\,, \qquad \mathbf{r}^{(e)} = \mathbf{r}_d^{(e)} - (\mathbf{K}_{\boldsymbol{\beta}\mathbf{q}}^{(e)})^T(\mathbf{K}_{\boldsymbol{\beta}\boldsymbol{\beta}}^{(e)})^{-1}\mathbf{r}_{\boldsymbol{\beta}}^{(e)}\,. \tag{5.45}$$

Since the parameters $\Delta\boldsymbol{\beta}_{(e)}$ are eliminated on the element level, the resulting EAS(14)m1 element has six dofs as specified by (5.31).

The global equations

$$\mathbf{K}_T\Delta\mathbf{q} = \Delta\mathbf{p} + \mathbf{j} \tag{5.46}$$

are formed from (5.44) and (5.45) in the course of standard aggregation,,

$$\mathbf{K}_T = \mathop{A}_{e=1}^{N_{elem}} \mathbf{K}_T^{(e)}\,, \quad \Delta\mathbf{p} = \mathop{A}_{e=1}^{N_{elem}} \Delta\mathbf{p}^{(e)}\,, \quad \mathbf{j} = \mathop{A}_{e=1}^{N_{elem}} \mathbf{j}^{(e)}\,, \quad \Delta\mathbf{q} = \begin{Bmatrix} \Delta\boldsymbol{q}_1 \\ \Delta\boldsymbol{q}_2 \\ \vdots \\ \Delta\boldsymbol{q}_{N_{node}} \end{Bmatrix}. \tag{5.47}$$

The global vector of increments of the generalized displacements $\Delta\mathbf{q}$ is built from $\Delta\boldsymbol{q}_a$ defined by $(5.31)_2$.

5.3. MATERIAL LAW

In this work we confine our considerations to a special case of the simplest material law (3.22). We generalize the classical constitutive equations for thin, isotropic, linearly elastic shells on the considered 6–field theory of shells. The equations read

$$\begin{Bmatrix} n^{11} \\ n^{22} \\ n^{12} \\ n^{21} \\ n^{1} \\ n^{2} \\ m^{11} \\ m^{22} \\ m^{12} \\ m^{21} \\ m^{1} \\ m^{2} \end{Bmatrix} = \begin{bmatrix} C & \nu & & & & & & & & & & \\ \nu & C & & & & & & & & & & \\ & & C(1-\nu) & & & & & & & & & \\ & & & C(1-\nu) & & & & & & & & \\ & & & & \frac{1}{2}\alpha_s C(1-\nu) & & & & & & & \\ & & & & & \frac{1}{2}\alpha_s C(1-\nu) & & & & & & \\ & & & & & & D & \nu & & & & \\ & & & & & & \nu & D & & & & \\ & & & & symm & & & & D(1-\nu) & & & \\ & & & & & & & & & D(1-\nu) & & \\ & & & & & & & & & & \alpha_t D(1-\nu) & \\ & & & & & & & & & & & \alpha_t D(1-\nu) \end{bmatrix} \begin{Bmatrix} \varepsilon_{11} \\ \varepsilon_{22} \\ \varepsilon_{12} \\ \varepsilon_{21} \\ \varepsilon_{1} \\ \varepsilon_{2} \\ \kappa_{11} \\ \kappa_{22} \\ \kappa_{12} \\ \kappa_{21} \\ \kappa_{1} \\ \kappa_{2} \end{Bmatrix} \tag{5.48}$$

where: h_0 is the shell thickness in the reference configuration, E is the Young modulus, ν denotes the Poisson ratio, $C = \dfrac{Eh_0}{1-\nu^2}$, $D = \dfrac{Eh_0^3}{12(1-\nu^2)}$. The shear factor α_s is well established on the grounds of theories of plates and shells. Here for numerical purposes the value $\alpha_s = 1$ has been used. The torsional factor α_t is the new material coefficient established for the present theory of shells. It should be viewed as an analogue of the shear factor α_s and must not be confused with the "penalty multiplier" notion used in reference [23] or [34], where the authors must have misunderstood the meaning of α_t.

It should be noted, however, that it was Reissner [12] who was the first to make an attempt to propose the constitutive equations for six-field shell theory. The constitutive equations for the drilling couples and, therefore, the value of α_t and its definition are still an open problem in the context of the discussed theory of shells. This

issue has been a topic of extensive studies in [14]-[16]. The studies and numerical simulations for $\alpha_t \in [10^{-10};10^{+10}]$ carried out there revealed that values of α_t from 0 to 1 have negligible influence on the values of displacements and on internal energy of the system. In this paper, for numerical simulations we chose $\alpha_t = 0.01$.

6. EXACT UPDATE PROCEDURE

The translation field $\boldsymbol{u}$ is updated in the additive manner

$$\boldsymbol{u}_{n+1}^{(i+1)} = \boldsymbol{u}_{n+1}^{(i)} + \Delta\boldsymbol{u}_{n+1}^{(i+1)}. \tag{6.1}$$

The update of the rotation tensor $\boldsymbol{Q}$ is more involving. As mentioned above, this update is performed here in the spatial representation. By making use of increment of the axial vector $\Delta\boldsymbol{w}_{n+1}^{(i+1)}$ at $(n+1)$ – configuration one gets

$$\boldsymbol{Q}_{n+1}^{(i+1)} = \Delta\boldsymbol{Q}_{n+1}^{(i+1)}\boldsymbol{Q}_{n+1}^{(i)} \quad \Rightarrow \quad \Delta\boldsymbol{Q}_{n+1}^{(i+1)} = \exp\left(\mathrm{ad}(\Delta\boldsymbol{w}_{n+1}^{(i+1)})\right). \tag{6.2}$$

The use of increment (correction) of the rotation vector $\Delta\boldsymbol{w}_{n+1}^{(i+1)}$ practically excludes the possibility of finding singular points of parametrization (A.4) at 2π, since in the Newton-Raphson scheme the convergence requirements rule out such large values of the axial vector.

The vector of parameters $\Delta\boldsymbol{\beta}_{(e)}$ of enhancing strains $\Delta\hat{\boldsymbol{e}}$, as an element of the linear space, is also updated in the additive way

$$\boldsymbol{\beta}_{n+1}^{(i+1)} = \boldsymbol{\beta}_{n+1}^{(i)} + \Delta\boldsymbol{\beta}_{n+1}^{(i+1)}. \tag{6.3}$$

Once the updates $\mathbf{u}_{n+1}^{(i+1)}$ and $\boldsymbol{\beta}_{n+1}^{(i+1)}$ are found, the associated strains are found from (4.1) where the compatible strains result from (3.13) and the enhancing part is found from (5.24). Then the corresponding stresses are determined from constitutive equation (4.9).

To follow the equilibrium paths, we use load control, displacement control or arc-length control technique, depending of the nature of the problem. The latter requires a brief comment. Namely, once we define in a standard way the arc length of the equilibrium path

$$\Delta s^2 = (\Delta \bar{\mathbf{q}}_{n+1})^T \Delta \bar{\mathbf{q}}_{n+1} + (\Delta \lambda_{n+1})^2 , \qquad \Delta s = const , \tag{6.4}$$

we note that due to different units and orders of magnitude of the elements of $\Delta \mathbf{q}$, there may be a problem in reasonable definition (in numerical sense) of (6.4). One of the ways to overcome this difficulty is the technique of selective elimination or scaling (see [33] and [35]).

Let N_{dof} be the total number of nodes and let $\mathbf{S} = \mathrm{diag}[s_1, s_2, ..., s_{N_{dof}}]$ be a diagonal matrix with elements s_p such as $0 \le s_p \le 1$, where $p = 1, 2, ..., N_{dof}$. The selective elimination (or scaling) may be then written as

$$\Delta \bar{\mathbf{q}}^{(i)} = \mathbf{S} \Delta \mathbf{q}^{(i)} . \tag{6.5}$$

In this paper, we have decided to assess the convergence by eliminating the rotational part of $\Delta \mathbf{q}^{(i)}$. This corresponds to calculations in the vector space (E) of configuration space $(E \times SO(3))$. The convergence check is performed by using the relative norm

$$\frac{\| \delta(\Delta \boldsymbol{u}) \|}{\| \Delta \boldsymbol{u} \|} < 0.001 . \tag{6.6}$$

Thereby we avoid difficulties associated with definition of convergence on $SO(3)$ group.

7. EXAMPLES

In order to assess the performance of the proposed 4-node semi-EAS finite element, we have solved several representative examples. The obtained results are compared with our solutions obtained with the help of other types of elements and with results reported in the literature.

7.1. SMOOTH PLATES AND SHELLS

7.1.1. Clamped membrane/plate

To gain knowledge about the influence of particular enhancing fields on the results, we analyze a (partially) clamped cantilever of length $L=10$, width $b=2$ and thickness $h_0=1.0$ (see Fig. 6). The support is located at $y=L$. The material parameters are: E = 1500, ν = 0.25. The analysis is confined to linear range. This is the popular benchmark example for membrane problems in the presence of mesh distorsions (Fig. 6a, 6b). It may be found for example in [36] or [37]. Here we propose additionally a variant for plate/shell elements (Fig. 6c, 6d). The computed translations of the point (a) are set in Table 1 with the reference solutions found according to the Bernoulli beam theory. The obtained results are very close to the reference solution though the accuracy deteriorates slightly in cases with irregular mesh.

This example shows that the enhancing fields for membrane or shear strains are selected properly, at least in the linear analysis. In particular, the element responds well to the constant bending load case (Fig. 6d).

7.1.2. Clamped skew plate

This example is taken from [38]. It is concerned with the skew clamped plate (see Fig. 7) subjected to uniformly distributed dead load. Due to the irregular mesh, this example enables the evaluation of the element in the presence of mesh distortions. In comparison to the previous example, here the geometrical nonlinearity (in small range) is taken into account. The problem has the following data: $L=300\,in$, $h=3\,in$, $E=3\times10^7\,lb/in$, $v=0.316$, $\beta=\{0^o,30^o,45^o\}$. In the computations originally, the double symmetry of the plate was utilized by discretizing one quarter of plate using 11 9-node Heterosis elements. Here we have adopted the original mesh for the 4-node elements (see Fig. 7). As the reference, the original results from [38] and solution obtained with the help of CAMe4 elements [15] with uniformly reduced integration (URI) are used. In addition, we present results for the square plate, found according to Levy's solution [38]. Figure 8 shows the obtained load-displacement paths for different value of angle β with respect to nondimensional load parameter $q^*=\frac{qL^4}{Eh^4}$ and corresponding nondimensional deflection parameter $w^*=\frac{w_C}{h}$ of the plate center. Good agreement between the reference results and the results obtained with the help of the proposed element has been obtained. The results show that at this level of nonlinearity, the element is insensitive to the mesh distortions. On examining the results from Figure 8 it can be noticed that the results produced by EAS(14)m1 element are slightly "soften" than the original solution.

7.1.3. Pinched cylinder

This example was originally presented in [39] with data: L = 3.04, R = 1.01, h_0 = 0.03, $E = 2.065\times10^7$, v = 0.3, P_{ref} = 10, $P(\lambda)=\lambda P_{ref}$ (see Fig. 9). In comparison with the

previous example, apart from geometrical nonlinearity here we deal with the single curvature problem.

Our initial interest in this example was caused by the remarkably good results of reported in [39] obtained with the aid of S16 (FI) element. These 16-node elements, as well as our CAMe16 (FI) elements, should produce locked results in coarse meshes. This effect was not observed in [39] even in 4×4 S16(FI) discretization of the whole structure. Reinterpretation of the problem data (load and discretization) as for symmetric part of the structure reveals the source of the mistake in [39].

In reference [40] the authors showed that coarse meshes used to solve this example might lead to the load-displacement path with artificial limit points. Their conclusion was that the solution with too coarse mesh required more time to solve. In our opinion more important is that such solutions are simply wrong, as they show the physical phenomena that do not exist. We believe that it is connected with too poor discretization which is not able to reproduce properly the deformation wave shortening with the growth of the load parameter.

To solve the problem we use the mesh of 16×16 EAS14m1 elements for half of the cylinder. As the reference solutions, we use the original results from [39] and those from [4]. Additionally, the solution obtained by making use of 16-node fully integrated displacement/rotation based CAMe16 elements is also presented. To track the equilibrium path we have used the arc-length method. We have carried out the analysis going with the value of vertical displacement beyond the value of radius $R = 1.01$. The results are compared in Fig. 10.

The results obtained using the proposed EAS(14)m1 element are in agreement with the reference solutions and are close to [4] what is worthy of note in the light of using the same concept to enhance the shear strains.

7.1.4. Pinched hemisphere with a hole

This benchmark problem (see Fig. 11) was proposed in [41] with data: $R=10$, $h_0=0.04$, $\alpha=18^o$, $E=6.825\times10^7$, $v=0.3$, $P_{ref}=10$, $P(\lambda)=\lambda P_{ref}$. We deal here with the small strains but with large translations and rotations. Additionally, here the geometry possesses two curvatures (cf. the previous examples). This popular example was the topic of extensive studies, see for instance references [4], [5], [7], [16], [17]. For example, in [16] the authors performed original analysis of the locking effect for various finite elements with full integration for increasing load level. It was found that for larger values of the load parameter the nonlinear convergence tends to deteriorate as a result of shortening length of deformation wave.

Here we compare our results obtained with the proposed EAS(14)m1 element used in meshes 8×8 and 16×16 elements with solutions reported in [4], [5], [7], [17]. The results obtained in 8×8 mesh are depicted in Fig. 12 and reported while the solutions with 16×16 mesh are shown in Fig. 13. The solutions obtained in 8×8 mesh are comparable to results of other authors, yet they are far from the reference solution CAMe16 8×8 (FI). When the mesh of 16×16 elements is used, our element gives the results practically identical to those of other researchers. However, in spite of using in the proposed EAS(14)m1 element the same enhancing fields for shear strains as in [4], we have not been able to reproduce the remarkably good results in 8×8 mesh from [4].

7.1.5. Twisted beam

The twisted beam subjected to point load (see Fig. 14) was proposed in [41]. The parameters of the problem are: $L=12$, $b=1.1$, angle of twist 90^o, $E=29\times10^6$,

$v = 0.22$. Originally, the thickness $h_0 = 0.32$ was used (see also [42] where the linear convergence has been studied), however, in [43] the thickness was reduced 100 times, i.e. $h_0 = 0.0032$, to invoke the locking effect. The latter reference contains also a remark that many elements fail when used to analyze the twisted beam problem.

Here we confine our attention to the variant with $h_0 = 0.0032$ subjected to load $P_Z = 1 \times 10^{-6}$, thereby we are able to compare our results with those presented in [24]. In that reference, the authors using the 2×24 mesh of 4-node hybrid stress and enhanced elements obtained in linear calculations the value of in-plane displacement to be 0.00522, which is almost identical to the analytical solution from [43] i.e. 0.005256. Our results of the linear convergence analysis are presented in Fig. 15 and in Table 2. The number of dofs does not include the enhancing variables as they are condensed on the element level. We obtained good approximation (0.005223) of the analytical result using 6×72 mesh of EAS(14)m1 elements. This value is also confirmed by the result (0.0052356) obtained using 3×24 mesh of CAMe16 (FI) elements, having the same number of dofs.

Having obtained unsatisfactory results using mesh 2×24 of EAS(14)m1 elements, we have carried out the nonlinear convergence analysis. Firstly we have used only displacement/rotation finite elements CAMe4, CAMe9 or CAMe16. A fragment of load-displacement path in the vicinity of the turning point depicted in Fig. 16 shows that the solutions converge typically as for underintegrated (URI) elements and are bound by CAMe16 (2×24) URI and CAMe16 (2×24) FI curves. Taking then these latter solution as the reference we proceeded with nonlinear convergence analysis using EAS(14)m1 element – see Fig. 17. By refining meshes we have found that even though our result in 6×72 mesh in the linear analysis converged to the analytical solution (and was identical

with the solution from [24]), in the nonlinear range our result, starting from the turning point, begins to differ from [24]. In Fig. 17 we also show the curve denoting trend in the *h*–convergence analysis. Coordinates of the turning points obtained in each discretization are set in Table 3. We have noticed negligible differences between the results obtained in 6×72 and 8×96 element meshes. Therefore, we have not pursued the analysis further. The eventual result from 8×96 mesh is shown in Fig. 18 and some representative values are reported in Table 4.

7.2. SHELLS WITH INTERSECTIONS

The examples analyzed in this section are spatial forms of large constructional stiffness resulting from their geometrical characteristics. The response of such structures is often complex i.e. there appears an interaction between local and global forms of the buckling. The load-displacement paths are usually complex and difficult to trace. We also deal with large deformations of translational and rotational type. Additionally, depending on the boundary conditions, especially in the case of large, almost rigid motions of large parts of the structure, either locking effect appears with full integration or spurious forms with reduced integration. The above features, in conjunction with the multi-branched character of geometry, make this type of examples very thorough and reliable tests for finite elements with the sixth degree of freedom.

7.2.1 Channel-section cantilever

We analyze the channel-section cantilever subjected to the concentrated force (see Fig. 19). This example takes its origin in [44] where it was analyzed as a simply supported beam with uniformly distributed (along the web) load. The authors tested this

example numerically within the moderate elasto-plastic strains, with the help of 4-node nonconforming flat finite element with six dofs at each node. Later, this example was undertaken in [15] in the original formulation as well as in [14], [15] and [17] in the cantilever setup with the concentrated force (see Fig. 19).

Here we analyze this example in two variants. The first one is the same as proposed in [14] while the second variant follows from [47]. Both variants differ from each other in their dimensions. It is of interests therefore to examine the qualitative differences in the behavior of both structures.

In the first variant, after [14], we use the following dimensions for the cantilever from Fig. 19: $L = 36$in, $a = 2$in, $b = 6$ in, $h_f = h_w = 0.05$in, $E = 10^7$lb/in^2, $v = 0.333$, $P_{ref} =$ 100lb, $P(\lambda) = \lambda P_{ref}$. Originally, in [14], the mesh of 5×9 of 9-node CAM elements (one element for the lower flange, three elements for the web, one element for the upper flange and nine elements along the length) with uniform reduced integration was used. Due to the coarse mesh, these solutions should be viewed rather as qualitative than quantitative ones. Later, this example was also analyzed in [9] and [22] as an elastic problem and in [23], [34], [45] as an elasto-plastic problem. In references [22] and [23] the mesh of 20×72 4-node elements was used for computations. In addition, we also present the solution from [46]. The results are compared in Fig. 20. As the reference, we provide the solution obtained using 14×36 16-node CAM elements with full integration. The results obtained with our own element EAS(14)m1 are in very good agreement with the results from [22] and [46]. Nevertheless, the results obtained with the aid of our 4-node element and taken from [22] remain slightly underestimated when compared to 14×36 16-node CAM solution. This may be attributed, to the authors' opinion, to different numbers of nodes along the cantilever length. Table 5 shows the numerical

results with boldface letters distinguishing values of control parameters that are the same for both formulations.

We have also noted some discrepancy between our solution in mesh 20×36 and results presented in [45] in the same mesh, despite the use of the analogical enhancement of the shearing strains. Yet, it is not clear from [45] how the orthogonal intersections are modeled with 5 dof element.

Figure 20 shows the influence of the mesh density on the locus of the limit point – the use of coarse mesh moves the limit point from $u \cong 0.25$ to $u \cong 0.5$. According to our animation of deformation before the limit point the cantilever responses in beam-like fashion, i.e. bending mode of deformation is prevailing. After passing the limit point there appears the torsional deformation. Moreover, just after passing the limit point there appear some local phenomena such as deformation waves in the vicinity of the support (see Fig. 21). These waves move along the beam during the deformation.

The second variant, as proposed in [47], has the following data L = 900cm, a = 10cm, b = 30cm, h_f = 1.6cm, h_w = 1.0cm, E = 21000kN/cm^2, ν = 0.3, P_{ref} = 1kN, $P(\lambda) = \lambda P_{ref}$. Fig. 22 and Table 6 show the comparison of our results obtained with EAS(14)m1 element and CAMe4 (URI) and CAMe16 (FI) elements with the original solution [47]. The discrepancies between results may stem from different ways of including the sixth degree of freedom. Namely, in [47] to model intersections three rotational dofs were used, and at the remaining parts of the structure the drilling rotation was eliminated. This is not the case in the present formulation where the drilling rotation is the natural consequence of the underlying theory of shells.

To summarize both variants of the cantilever it should be noted that the change of parameters in the second case has changed the qualitative response of the structure. In

particular, in the second variant there is no limit point on the deformation path. The visualization of the deformation (see [47]) reveals that the local phenomena do not occur here as in the first variant - the response of the cantilever in the second variant is more beam-like. With the parameters proposed in [47] the example lost its "shell-like" character.

7.2.2 Twisted T-shaped cantilever

Another example is the twisted T-shaped cantilever from Fig. 23. The importance of this example is that it generalizes the twisted (smooth) beam (see Example 7.1.5). The present example has already been studied in [48] in the context of formulating time-stepping algorithm for 6-field theory of shells. The authors selected data so that the moment of inertia of the cross-section about x–axis is equal to that about z–axis which yields: $H=10$, $B=14.0112$, $h_0=0.25=const$. The remaining parameters are: $L=50$, $\alpha=90^o$, $E=2\times10^7$, $\nu=0.3$, $P_{X,ref}=1000$, $P_{Z,ref}=1000$, $P(\lambda)=\lambda P_{ref}$.

To start with, we have carried out the linear convergence analysis (see Table 7). For further nonlinear calculations, we have selected only one load case $P_{X,ref}=1000$. The results are depicted in Fig. 24 and set in Table 8. On examining the load-deformation paths from Fig. 24 with connection to Table 7 it is seen that though the linear results obtained with meshes EAS(14)m1 $(12+6)\times30$ and CAMe16 $(4+2)\times10$ (FI) are reasonable, the same is not true in the nonlinear solutions. This effect has already been mentioned in this paper. With more refined meshes both results coincide in the nonlinear calculations.

7.2.3 Critical load of torsional buckling of I-beam column

This example is concerned with the torsional buckling of the compressed I-beam column. The problem is of practical significance as the open thin-walled members are prone to stability loss. Hence, the knowledge about the critical load is of importance from the engineering viewpoint. Geometry and the FEM setup are depicted in Fig. 25. The example has the following data: $E = 2.1\times10^6 kN/m^2$, $v = 0.3$, $L = 8m$, $B = H = 0.2m$, $h_0 = 0.01m$.

In the FEM analysis, due to bisymmetry of the column, only a half-length of the column is discretized. In the non-linear stability analysis, a one-parameter dead load of the form $P(\lambda) = \lambda P_{ref}$ (where $P_{ref} = q_{ref} A = 1MN$ is uniformly distributed over the cross-section) is used. As the imperfection load, the torsional moment $M_{impf} = 1Nm$ is applied at point (c) on the longitudinal axis (see Fig. 25). Since we are concerned with the torsional buckling, the boundary conditions are so employed that the beam may only move and rotate along the longitudinal axis.

The path with imperfection has been traced using the load control and the arc-length control techniques until reaching neighborhood of the secondary path, where the imperfection moment has been removed yielding the jump on the secondary path. Then using from that point the displacement control technique until the control displacement *u* at the point *j* was close to zero, the beam has been restored to its symmetric state at the bifurcation point yielding the load multiplier of torsional buckling λ_{CR}. The results obtained with the aid of EAS(14)m1 element are compared with solutions from CAMe16(FI) elements in Table 9. Notation (*a*+*b*+*c*)×(*d*) stands for number of elements used to model the structure (lower flange + web + upper flange) × (half of the length).

From Table 9 it is seen that the obtained results depend on the number of elements used along the length of the beam. With more refined meshes the value of critical load

of torsional buckling converges to about 2.02 MN, which is smaller than the result obtained with the aid of theory of thin-walled members [49].

8. CONCLUSIONS

In this paper we have presented an extension of EAS technique to 6–field theory of shells with asymmetric strain measures in geometrically nonlinear static problems. We have elaborated new 4–node C^0 finite element for shell structures undergoing unlimited translations and rotations. The enhancing field, accommodating the lack of symmetry of membrane strains, has been proposed for stretching strains (including shearing components). The resulting finite element, denoted EAS(14)m1, has fourteen enhancing parameters. From the numerical simulations presented, the following attributes of the elaborated element are worth mentioning

- Combination of EAS technique and asymmetric strain measures is possible.
- In the geometrically linear analysis the proposed EAS element possesses good coarse mesh accuracy. In particular, the element works well in case of the constant bending moments.
- In geometrically nonlinear problems of flat geometry, the proposed element also works well, though the results seem a bit soften than the reference solutions. In cases of curved geometries, the results produced by the element are almost identical to the solutions reported by other authors or obtained with different element formulations. We noted, however, that in one of the solved examples our element exhibited slower convergence rate than those obtained by other researchers.

- We have successfully employed the EAS element in the analysis of shell structures with irregularities of geometry, i.e. with orthogonal intersections. The attained accuracy is comparable to other solutions known from literature and, in particular, to the 16–node displacement/rotation based elements developed within the same shell theory.
- The obtained results confirm the observation from [24] that the behavior and the convergence of results in the nonlinear analysis may differ from that in the linear analysis. This is true given the fact that in nonlinear calculations we deal here with propagation of the deformation wave. Hence, in order to describe such phenomenon properly we need a sufficiently dense mesh. Therefore, one may question the precision of the results obtained in coarse meshes sometimes reported in literature.

Considering the above, the proposed enhancing fields are correctly adopted for the needs of theory of shells with asymmetric strain measures and are efficient in elimination of the membrane and shear locking. Yet, we are aware that the enhancement proposed here is "rich" in the sense that it generates the element stiffness matrix of large size. The search for more efficient enhancement is being carried out. In particular, we investigate the combination of EAS technique for membrane strains with ANS approach for shear locking. Some promising results have already been obtained (see [50]).

ACKNOWLEDGEMENTS

The financial support of the Polish State Committee for Scientific Research under Grant No 5 T07 A 00825 is gratefully acknowledged.

Wojciech Witkowski is awarded by Foundation for Polish Science.

APPENDIX 1 PARAMETRIZATION OF ROTATIONS

In this paper, parametrization of the rotations is based on the finite rotation vector in the spatial representation. Let E denote the three-dimensional vector space and let $\boldsymbol{Q}$ be a proper orthogonal tensor, such as for example $\boldsymbol{T}_0$ in (2.9).

At the point $\boldsymbol{Q}=\mathbf{1}$ of $SO(3)=\left\{\boldsymbol{Q}:\boldsymbol{Q}^T\boldsymbol{Q}=\boldsymbol{Q}\boldsymbol{Q}^T=\mathbf{1},\det(\boldsymbol{Q})=+1\right\}$ there exists a tangent space $so(3)$ of skew-symmetric tensors defined by

$$so(3)=\{\boldsymbol{W}:\boldsymbol{W}^T=-\boldsymbol{W}\}, \tag{A.1}$$

which is isomorphic with the vector space E. A map $\mathrm{ad}(.)$ understood here as

$$\mathrm{ad}:E\to so(3),\qquad \boldsymbol{w}\to\boldsymbol{W}=\mathrm{ad}(\boldsymbol{w}),\qquad \boldsymbol{W}\to\boldsymbol{w}=\mathrm{ad}^{-1}(\boldsymbol{W}), \tag{A.2}$$

where $\boldsymbol{w}$ is an axial vector of $\boldsymbol{W}$. In a given base one gets from (A.2)

$$[W_{ij}]=\begin{bmatrix}0 & -w_3 & w_2\\ w_3 & 0 & -w_1\\ -w_2 & w_1 & 0\end{bmatrix},\qquad [w_i]=\begin{bmatrix}w_1\\ w_2\\ w_3\end{bmatrix},\qquad [w_i]\to[W_{ij}]=\mathrm{ad}([w_i]). \tag{A.3}$$

The tensor $\boldsymbol{Q}\in SO(3)$ in the so-called canonical parametrization takes the form

$$\boldsymbol{Q}=\mathbf{1}+a\boldsymbol{W}+b\boldsymbol{W}^2, \tag{A.4}$$

where

$$\boldsymbol{W}=\mathrm{ad}(\boldsymbol{w})\in so(3),\qquad a=\frac{\sin w}{w},\qquad b=\frac{1-\cos w}{w^2},\qquad w=\|\boldsymbol{w}\|=\sqrt{\boldsymbol{w}\cdot\boldsymbol{w}}. \tag{A.5}$$

The relations reciprocal to (A.4) are given by

$$\cos w=\frac{1}{2}(tr\boldsymbol{Q}-1),\qquad \Rightarrow\qquad w=\arccos\left(\frac{1}{2}(tr\boldsymbol{Q}-1)\right), \tag{A.6}$$

$$2\sin w(\mathrm{ad}\boldsymbol{w}) = \boldsymbol{Q} - \boldsymbol{Q}^T \quad \Rightarrow \quad \boldsymbol{w} = \frac{1}{2\sin w}\mathrm{ad}^{-1}(\boldsymbol{Q} - \boldsymbol{Q}^T)\,. \tag{A.7}$$

In the spatial representation the variation $\delta\boldsymbol{Q}$ defined as the directional derivative at $\boldsymbol{Q}$ in direction $\mathrm{ad}(\boldsymbol{w})$, reads

$$\delta\boldsymbol{Q}[\boldsymbol{Q};\mathrm{ad}(\boldsymbol{w})] \equiv \frac{d}{d\eta}\boldsymbol{Q}(\eta)\Big|_{\eta=0} = \frac{d}{d\eta}\exp(\mathrm{ad}\eta\boldsymbol{w})\Big|_{\eta=0}\boldsymbol{Q} = \mathrm{ad}\boldsymbol{w}\,\boldsymbol{Q}\,. \tag{A.8}$$

The rotations are accumulated as follows. Let $\boldsymbol{Q} \in SO(3)$ send a fixed orthogonal frame $\{\boldsymbol{t}_i^0, i = 1,2,3\}$ to another orthogonal frame $\{\boldsymbol{t}_i, i = 1,2,3\}$

$$\boldsymbol{t}_i = \boldsymbol{Q}\boldsymbol{t}_i^0\,. \tag{A.9}$$

Let us consider some increment ${}^{\Delta}\boldsymbol{Q} = \Delta\boldsymbol{Q} \in SO(3)$ of the rotation that carries the frame $\{\boldsymbol{t}_i\}$ to some updated frame $\{{}^{\Delta}\boldsymbol{t}_i\}$. In the spatial representation, which is used in this paper, such an increment is expressed by

$${}^{\Delta}\boldsymbol{Q} = \Delta\boldsymbol{Q}\boldsymbol{Q}\,, \quad {}^{\Delta}\boldsymbol{t}_i = \Delta\boldsymbol{Q}\boldsymbol{t}_i = \Delta\boldsymbol{Q}\boldsymbol{Q}\boldsymbol{t}_i^0\,, \quad \Delta\boldsymbol{Q} = \exp(\mathrm{ad}\,\Delta\boldsymbol{w})\,. \tag{A.10}$$

Discussion on the material representation may found, for example in [28].

Figure Captions.

Figure 1. The shell-like body

Figure 2. An arbitrary part of the shell-like body in the reference configuration

Figure 3. Resultant forces and couples

Figure 4. Formal, local, parametrization of *M*

Figure 5. Physical components of resultant forces and moments

Figure 6. Partially clamped cantilever membrane/plate: geometry, load, discretizations

REFERENCES

[1] Ahmad S, Irons BM, Zienkiewicz OC. Analysis of thick and thin shell structures by curved finite elements. *Int. J. Num. Meth. Engng.* 1970; **2**: 419-451.

[2] Andelfinger U, Ramm E. EAS elements for two-dimensional, three-dimensional, plate and shell structures and their equivalence to HR elements. *Int. J. Num. Meth. Engng* 1993; **36**: 1311-1337.

[3] Cesar de Sa JMA, Jorge RMN, Valente RAF, Areias PMA. Development of shear locking-free shell elements using an enhanced assumed strain formulation. *Int. J. Num. Meth. Engng* 2002; **53**: 1721-1750.

[4] Valente RAF, Jorge RMN, Cardoso RPR., César de Sa JMA, Grácio JJA. On the use of an enhanced transverse shear strain shell element for problems involving large rotations. *Comput. Mech.* 2003; **30**: 286-296.

[5] Simo JC, Fox DD, Rifai MS. On a stress resultant geometrically exact shell model. Part III: Computational aspects of the nonlinear theory. *Comp. Meth. Appl. Mech. Engng*, 1990; **79**: 21-70.

[6] Büchter N, Ramm E. Shell theory versus degeneration – a comparison in large rotation finite elements analysis. *Int. J. Numer. Methods Engng* 1992; **34**: 39-59.

[7] Sansour C, Bufler H. An exact finite rotation shell theory, its mixed variational formulation and its finite element implementation. *Int. J. Num. Meth. Engng* 1992; **34**: 73-115.

[8] Ibrahimbegović A. Stress resultant geometrically nonlinear shell theory with drilling rotations - Part I: A consistent formulation. *Comp. Meth. Appl. Mech. Engng*. 1994; **118**: 265-284.

[9] Ibrahimbegović A, Frey F. Stress resultant geometrically nonlinear shell theory with drilling rotations - Part II: Computational aspects. *Comp. Meth. Appl. Mech. Engng*, 1994; **118**: 285-308.

[10] Wiśniewski K. A shell theory with independent rotations for relaxed Biot stress and right stretch strain. *Computational Mechanics.* 1998; **21**: 101-122.

[11] Wiśniewski K, Turska E. Warping and in-plane twist parameter in kinematics of finite rotation shells. *Comp. Meth. Appl. Mech. Engng.* 2001; **190**: 5739-5758.

[12] Reissner E. Linear and nonlinear theory of shells. In: *Thin Shell Structures* (eds: Fung Y.C., Sechler E.E.). Englewood Cliffs: Prentice-Hall, 1974; 29-44.

[13] Libai A, Simmonds JG. *The Nonlinear Theory of Elastic Shells.* Cambridge University Press, 1998.

[14] Chróścielewski J, Makowski J, Stumpf H. Genuinely resultant shell finite elements accounting for geometric and material non-linearity, *Int. J. Numer. Methods Engng.* 1992; **35**: 63–94.

[15] Chróścielewski J. *Family of C^0 finite elements in six parameter nonlinear theory of shells*. Gdansk University of Technology Publishers, Civil Eng Series, 540(LIII), Gdansk, Poland 1996

[16] Chróścielewski J, Makowski J, Stumpf H. Finite element analysis of smooth, folded and multi-shell structures. *Comp. Meth. Appl. Mech. Engng*, 1997; **141**: 1-46.

[17] Chróścielewski J. Makowski J. Pietraszkiewicz W. *Statics and Dynamics of Multifold Shells: Nonlinear Theory and Finite Element Method*. (in Polish). IPPT PAN: Warsaw, 2004.

[18] Bathe KJ, Dvorkin E. A formulation of general shell elements - the use of mixed interpolation of tensorial components. *Int. J. Num. Meth. Engng*, 1986; **22**: 697-722.

[19] Simo JC, Rifai MS. A class of mixed assumed strain methods and the methods of incompatible modes. *Int. J. Num. Meth. Engng*, 1990; **29**: 1595-1638.

[20] Braess D. Enhanced assumed strain elements and locking in membrane problems *Comput. Methods. Appl. Mech. Engrg,* 1998*;* **165**: 155-174.

[21] Taylor RL, Beresford PJ, Wilson EL. A non – conforming element for stress analysis. *Int. J. Num. Meth. Engng*, 1976; **10**, 1211-1219.

[22] Betsh P, Gruttmann F, Stein E. A 4–node shell element for the implementation of general hyperelastic 3D–elasticity at finite strains. *Comput. Methods. Appl. Mech. Engrg*, 1996; **130**: 57-79.

[23] Eberlein R, Wriggers P. Finite element concepts for finite elastoplastic strain and isotropic stress response in shells: theoretical and computational analysis. *Comp. Meth. Appl. Mech. Engng*, 1999; **171**: 243-279.

[24] Sansour C, Kollmann FG. Families of 4-node and 9-node finite elements for a finite deformation shell theory. An assessment of hybrid stress, hybrid strain and enhanced strain elements. *Comput. Mech.,* 2000; **24**: 435-447.

[25] Stuelpnagel J. On the parameterization of the three-dimensional rotation group. *SIAM Review* 1964; **6**: 422-430.

[26] Pietraszkiewicz W, Badur J. Finite rotations in the description of continuum deformation. *Int. J. Engineering Sci*., 1983; **21**: 1097-1115.

[27] Cardona A, Geradin M. A beam finite element non-linear theory with finite rotations. *Int. J. Num. Meth. Engng*, 1988; **26**: 2403-2438.

[28] Ibrahimbegović A. On the choice of finite rotation parameters. *Comp. Meth. Appl. Mech. Engng*, 1997; **149**: 49-71.

[29] Smoleński WM. Statically and kinematically exact nonlinear theory of rods and its numerical verification. *Comp. Meth. Appl. Mech. Engng.* 1999; **178**: 89-113.

[30] Betsh P, Menzel A, Stein E. On the parameterization of finite rotations in computational mechanics. A classification of concepts with application to smooth shells. *Comput. Methods. Appl. Mech. Engrg*, 1998; **155**: 273-305.

[31] Simmonds JG. The nonlinear thermodynamical theory of shells: Descent from 3-dimensions without thickness expansions. *Flexible Shells, Theory and Applications*. Axelrad E.L., Emmerling F.A. (eds), Springer-Verlag, 1984; 1-11.

[32] Chróścielewski J, Makowski J, Pietraszkiewicz W. Non-linear dynamics of flexible shell structures. *Comp. Assisted Mech. Engng Sci.* 2002; **9**: 341-357.

[33] Chróścielewski J, Nolte LP. Strategien zur Lösung nichtlinearer Probleme der Strukturmechanik und ihre modulare Aufbereitung im Konzept MESY. *Mitt. Institut für Mechanik.* Ruhr-Universität, Bochum, 1985; **48**.

[34] Tan XG, Vu-Quoc L. Efficient and accurate multilayer solid-shell element: Non-linear materials at finite strain. *Int. J. Num. Meth. Engng*, 2005; **63**: 2124–2170, DOI: 10.1002/nme.1360

[35] Schweizerhof K. *Quasi–Newton Verfahren und Kurvenverfolgungsalgorithmen für die Lösung nichtlinearer Gleichungssysteme in der Strukturmechanik*. Institut für Baustatik, 1989; **9**, Universität Fridericiana Karlsruhe.

[36] Pian THH, Sumihara K. Rational approach for assumed stress finite elements. *Int. J. Num. Meth. Engng*, 1984; **20**: 1685-1695.

[37] Piltner R, Taylor RL. A systematic construction of B-bar functions for linear and non-linear mixed-enhanced finite elements. *UCB/SEMM Report 96/02,* University of California at Berkeley, 1996.

[38] Pica A, Wood RD, Hinton E. Finite element analysis of geometrically nonlinear plate behaviour using a Mindlin formulation. *Comp. Struct.*, 1980; **11**: 203-215

[39] Stander N, Matzenmiller A, Ramm E. An assessment of assumed strain methods in finite rotation shell analysis. *Eng. Comput.*, 1989; **6**: 58-66.

[40] Crisfield MA, Peng X. Instabilities induced by coarse meshes for a nonlinear shell problem. *Eng. Comput*., 1996; **13**: 110-114.

[41] MacNeal RH, Harder RL. A proposed standard set of problems to test finite element accuracy. *Finite Elem. Anal. Design*, 1985; **1**: 3-20.

[42] TAYLOR R.L. [1988], Finite element analysis of linear shell problems. In: Whiteman J.R (ed.), *The Mathematics of Finite Elements and Applications VI*, 191-203. Academic Press, London.

[43] Belytschko T, Wong BL, Stolarski H. Assumed strain stabilization procedure for the 9-node Lagrange shell element. *Int. J. Num. Meth. Engng*, 1989; **28**: 385-414.

[44] Lee HP, Haris PJ. Post-buckling strength of thin-walled members. *Comp. Struct.*, 1979; **10**: 689-702.

[45] Valente RAF, Parente MPL, Jorge RMN, César de Sa JMA, Grácio JJA. Enhanced transverse shear strain shell formulation applied to large elasto-plastic deformation problems. *Int. J. Num. Meth. Engng*, 2005; **62**: 1360–1398, DOI: 10.1002/nme.1231

[46] private communication, results based on: Wagner W, Gruttmann F. A robust non-linear mixed hybrid quadrilateral shell element. *Int. J. Num. Meth. Engng*, 2005; **64**: 635-666, DOI: 10.1002/nme.1387

[47] Wagner W, Gruttmann F. A robust non-linear mixed hybrid quadrilateral shell element. *Int. J. Num. Meth. Engng*, 2005; **64**: 635-666, DOI: 10.1002/nme.1387

[48] Lubowiecka I, Chróścielewski J. On dynamics of flexible branched shell structures undergoing large overall motion using finite elements. *Comp. Struct.*, 2002; **80**: 891-898.

[49] Thimoshenko SP, Gere JM. *Theory of elastic stability*. Mc Graw-Hill: New York, II ed. 1961.

[50] Chróścielewski J, Lubowiecka I, Witkowski W. *4-node EAS-ANS strain element in 6-field nonlinear theory of shells*. In: Shell structures: Theory and applications : Proceedings of the 8th SSTA Conference: Jurata, Poland, 12-14 October 2005,

Pietraszkiewicz W, Szymczak C (eds), - London: Taylor & Francis/Balkema, 2005. ISBN 0-415-38390-0, s: 451-457.

Table 1. Clamped membrane/plate, displacements of point (a)

	Load case			
	A	**B**	**C**	**D**
displacement	$u_{(a)}$	$u_{(a)}$	$w_{(a)}$	$w_{(a)}$
*Reference**	**100.000**	**102.600**	**268.660**	**20.000**
Element	*REGULAR MESH*			
EAS(14)m1	99.900	101.57	262.06	19.818
	IRREGULAR MESH			
EAS(14)m1	95.069	97.136	264.03	20.533

*according to Bernoulli beam theory

Table 2. Twisted beam, linear convergence analysis

Mesh (*nodes*) / *Result*	3×25	5×49	7×73	9×97
Belytschko et al.[1989]	*reference*: 0.005256			
4-node elements				
Sansour and Kolmann [2000]	0.00522	—	—	—
EAS(14)m1	0.0040746	0.0051192	0.0052230	0.0052418
16-node elements				
CAMe16 (2×24)	—	—	0.0052356	

Table 3. Twisted beam, nonlinear analysis, coordinates of the turning point

	EAS(14)m1		CAMe16 FI	
Mesh (nodes)	P_Z	u	P_Z	u
3×25	0.00348911	2.45071	—	—
5×49	0.00300835	2.20462	—	—
7×73	0.00296481	2.17898	0.00303012	2.19422
9×97	0.00292308	2.17351	—	—

Table 4. Twisted beam, nonlinear analysis, some representative values

CAMe16 (2×24) (FI)				EAS14m1 (8×96)			
P_z	$-u$	v	w	P_z	$-u$	v	w
2.72911e–04	5.0000e–01	–1.0944e–01	1.4092e+00	2.72076e–04	5.0000e–01	–1.0922e–01	1.4075e+00
5.78864e–04	1.0000e+00	–4.5506e–01	2.8552e+00	5.77085e–04	1.0000e+00	–4.5448e–01	2.8529e+00
9.81323e–04	1.5000e+00	–1.1135e+00	4.4120e+00	9.79042e–04	1.5000e+00	–1.1144e+00	4.4137e+00
1.73438e–03	2.0000e+00	–2.4262e+00	6.3546e+00	1.74384e–03	2.0000e+00	–2.4523e+00	6.3874e+00
1.87743e–03	2.0500e+00	–2.6544e+00	6.6180e+00	1.89484e–03	2.0500e+00	–2.6933e+00	6.6638e+00
2.35728e–03	2.1537e+00	–3.3505e+00	7.3370e+00	2.45456e–03	2.1527e+00	–3.4939e+00	7.4760e+00
2.91717e–03	2.1931e+00	–4.0349e+00	7.9454e+00	2.77445e–03	2.1715e+00	–3.8891e+00	7.8281e+00
3.07715e–03	2.1942e+00	–4.2081e+00	8.0867e+00	2.93441e–03	2.1736e+00	–4.0714e+00	7.9814e+00
3.23713e–03	2.1922e+00	–4.3724e+00	8.2165e+00	3.09437e–03	2.1720e+00	–4.2442e+00	8.1219e+00
3.79708e–03	2.1668e+00	–4.8858e+00	8.5980e+00	3.25433e–03	2.1673e+00	–4.4082e+00	8.2511e+00
4.54703e–03	2.1070e+00	–5.4509e+00	8.9803e+00	4.13420e–03	2.1052e+00	–5.1760e+00	8.8079e+00
5.59548e–03	2.0050e+00	–6.0707e+00	9.3608e+00	4.68500e–03	2.0500e+00	–5.5643e+00	9.0627e+00
7.70772e–03	1.8000e+00	–6.9442e+00	9.8395e+00	6.98846e–03	1.8000e+00	–6.7109e+00	9.7294e+00
1.33176e–02	1.4000e+00	–8.1792e+00	1.0427e+01	1.17788e–02	1.4000e+00	–7.9492e+00	1.0336e+01
2.41266e–02	1.0025e+00	–9.1866e+00	1.0853e+01	1.96495e–02	1.0289e+00	–8.8894e+00	1.0741e+01
3.71766e–02	7.7169e–01	–9.7444e+00	1.1076e+01	2.99995e–02	7.7499e–01	–9.4972e+00	1.0988e+01

Table 5. Channel-section cantilever (variant 1), some representative values

CAMe16 (4+6+4)×36 (FI)				EAS14m1 (4+12+4)×72			
λ	u	$-v$	$-w$	λ	u	$-v$	$-w$
0.0	0.0000	0.0000	0.0000	**0.0**	0.0000	0.0000	0.0000
0.2	2.4564e–02	2.9690e–03	5.3276e–02	**0.2**	2.4489e–02	2.9399e–03	5.3225e–02
0.4	5.2699e–02	6.1359e–03	1.1783e–01	**0.4**	5.2537e–02	6.0759e–03	1.1770e–01
0.6	8.6438e–02	9.5435e–03	1.9838e–01	**0.6**	8.6155e–02	9.4499e–03	1.9810e–01
0.8	1.2966e–01	1.3239e–02	3.0303e–01	**0.8**	1.2916e–01	1.3106e–02	3.0242e–01
1.0	1.9074e–01	1.7228e–02	4.4723e–01	**1.0**	1.8973e–01	1.7043e–02	4.4583e–01
1.1	2.3383e–01	1.9252e–02	5.4464e–01	**1.1**	2.3221e–01	1.9037e–02	5.4212e–01
1.11466	2.4140e–01	1.9537e–02	5.6169e–01	1.12747	2.4643e–01	1.9561e–02	5.7410e–01
1.14588	2.6758e–01	1.9909e–02	6.3773e–01	1.15640	2.8066e–01	1.9583e–02	6.8452e–01
1.13975	2.8616e–01	1.9076e–02	7.2201e–01	1.14814	2.9770e–01	1.8619e–02	7.6278e–01
1.11591	3.2276e–01	1.6269e–02	8.9368e–01	1.13363	3.2059e–01	1.6871e–02	8.6823e–01
1.10785	**3.3500e–01**	1.5118e–02	9.4908e–01	1.12444	**3.3500e–01**	1.5586e–02	9.3281e–01
1.09839	**3.5000e–01**	1.3596e–02	1.0152	1.11527	**3.5000e–01**	1.4127e–02	9.9819e–01
1.07073	**4.0000e–01**	7.8050e–03	1.2225	1.08860	**4.0000e–01**	8.5634e–03	1.2028
1.00180	**6.0000e–01**	–2.2436e–02	1.9009	1.02336	**6.0000e–01**	–2.0606e–02	1.8713
0.97146	**8.0000e–01**	–5.8720e–02	2.4298	0.9946	**8.0000e–01**	–5.5850e–02	2.3922
0.95809	**1.0000**	–9.8497e–02	2.8721	0.98260	**1.0000**	–9.4550e–02	2.8270
0.95183	**1.4000**	–1.8464e–01	3.5951	0.978357	**1.4000**	–1.7855e–01	3.5365
0.95586	**1.8000**	–2.7695e–01	4.1795	0.984610	**1.8000**	–2.6881e–01	4.1088
0.96427	**2.2000**	–3.7461e–01	4.6770	0.99592	**2.2000**	–3.6410e–01	4.5915

Table 6. Channel-section cantilever (variant 2), some representative values

CAMe16 (4+8+4)×36 (FI)				EAS14m1 (4+12+4)×72			
P	*u*	*−v*	*−w*	*P*	*u*	*−v*	*−w*
2.0	2.9784	0.065037	0.54108	*2.0*	2.9760	0.064967	0.53648
4.0	6.0276	0.1201	1.8041	*4.0*	6.0214	0.11997	1.7858
6.0	9.3627	0.15666	5.0186	*6.0*	9.3438	0.15682	4.9459
8.0	16.531	-0.10533	20.978	*8.0*	16.208	-0.080111	20.195
8.2	19.234	-0.32128	26.613	*8.2*	18.666	-0.27134	25.461
8.5	26.871	-1.0552	39.115	*8.5*	25.672	-0.93167	37.414
9.0	46.824	-3.3933	60.378	*9.0*	45.285	-3.200	59.138
10.0	84.163	-8.8482	83.116	*10.0*	82.829	-8.6484	82.668
14.0	185.75	-30.821	106.66	*14.0*	184.81	-30.613	106.84
16.0	223.24	-41.986	109.16	*16.0*	222.36	-41.759	109.70
20.0	286.29	-65.271	110.46	*20.0*	285.40	-64.944	110.76

Table 7. Twisted T-shaped cantilever, linear convergence analysis

Discretization \ *Displacements*		$P_{X,ref}=1000$			$P_{Z,ref}=1000$		
		u(a)	*v*(a)	*w*(a)	*u*(a)	*v*(a)	*w*(a)
(2+1) ×5	EAS(14)m1	0.15812	0.0018519	–0.040874	–0.041199	–0.015200	0.081936
(6+3)×15	EAS(14)m1	0.15173	0.0013349	–0.026003	–0.026003	–0.0012001	0.095162
(12+6)×30	EAS(14)m1	0.15718	0.0013416	–0.024884	–0.024884	–0.0012470	0.097961
(24+12)×60	EAS(14)m1	0.15820	0.0013343	–0.024501	–0.024501	–0.0012806	0.098709
(2+1)×5	CAMe16 (FI)	0.13651	0.0011721	–0.023632	–0.023632	–0.0010145	0.087561
(4+2)×10	CAMe16 (FI)	0.15597	0.0013331	–0.024582	–0.024582	–0.0012590	0.097407
(8+4)×20	CAMe16 (FI)	0.15835	0.0013302	–0.024379	–0.024379	–0.0013015	0.098886

Table 8. Twisted T-shaped cantilever, nonlinear analysis, some representative values

CAMe16 (8+4)×20 (FI)				EAS14m1 (24+12)×60			
λ	u	v	w	λ	u	v	w
0.00000e+00	0.0000e+00	0.0000e+00	0.0000e+00	0.00000e+00	0.0000e+00	0.0000e+00	0.0000e+00
5.00000e+00	8.6618e-01	1.7916e–03	1.1258e–01	5.00000e+00	8.6437e-01	1.7377e–03	1.1364e–01
1.00000e+01	1.9989e+00	3.0985e–02	1.9455e–01	1.00000e+01	1.9787e+00	3.0025e–02	1.9922e–01
1.22164e+01	3.1842e+00	1.0078e–01	2.8898e–01	1.25704e+01	3.1688e+00	9.8104e–02	2.8710e–01
1.30519e+01	4.7384e+00	2.4801e–01	4.8789e–01	1.34741e+01	4.7245e+00	2.4489e–01	4.8565e–01
1.36829e+01	7.4242e+00	6.3348e–01	8.6721e–01	1.40982e+01	7.4130e+00	6.3125e–01	8.7256e–01
1.39112e+01	9.3153e+00	1.0079e+00	1.1692e+00	1.42887e+01	9.3073e+00	1.0088e+00	1.1929e+00
1.39846e+01	1.0170e+01	1.2054e+00	1.3157e+00	1.43783e+01	1.0588e+01	1.3145e+00	1.4279e+00
1.36326e+01	8.5903e+00	8.4866e–01	1.0653e+00	1.35643E+01	6.9995E+00	5.5115E-01	8.4744E-01
1.27755e+01	6.0903e+00	4.0821e-01	7.3007E-01	1.31209E+01	5.9995E+00	3.9379E-01	7.2459E-01
1.18491e+01	4.9542e+00	2.5134e–01	6.4655e–01	1.19555e+01	4.7583e+00	2.2465e–01	6.4879e–01
1.13895E+01	4.7698E+00	2.2355E-01	6.8436E-01	1.16304e+01	4.6792e+00	2.1094e–01	6.8508e–01
1.09884E+01	5.2291E+00	2.6498E-01	8.9130E-01	1.13341e+01	4.8302e+00	2.2088e–01	7.8037e–01
1.09901e+01	5.7291e+00	3.2404e–01	1.0377e+00	1.12157e+01	5.2502e+00	2.6376e–01	9.2421e–01
1.11360e+01	6.6291e+00	4.4884e–01	1.2719e+00	1.13345e+01	6.3502e+00	4.0448e–01	1.2222e+00
1.14405E+01	7.9291E+00	6.6723E-01	1.5813E+00	1.16808e+01	7.8502e+00	6.4882e–01	1.5739e+00
1.19496e+01	9.9291e+00	1.0888e+00	2.0237e+00	1.24256e+01	1.0850e+01	1.3095e+00	2.1912e+00
1.27110e+01	1.2929e+01	1.9176e+00	2.6371e+00	1.31353e+01	1.3850e+01	2.2016e+00	2.7260e+00
1.42809e+01	1.8929e+01	4.3181e+00	3.5786e+00	1.45425e+01	1.9850e+01	4.7235e+00	3.3919e+00

Table 9. Critical load of torsional buckling
Discretizations for half-length of the beam

element EAS(14)m1	*Load multiplier* [MN]		element CAMe16
	λ	λ	
EAS14m1(4+4+4)×15	2.0478	———	———
EAS14m1(4+4+4)×30	2.0356	———	———
EAS14m1(4+4+4)×60	2.0349	———	———
EAS14m1(6+6+6)×120	2.0263	2.0344	CAMe16(2+2+2)×40
EAS14m1(12+12+12)×240	2.0233	2.0249	CAMe16(4+4+4)×80
	Theory of thin walled members **2.0472**		

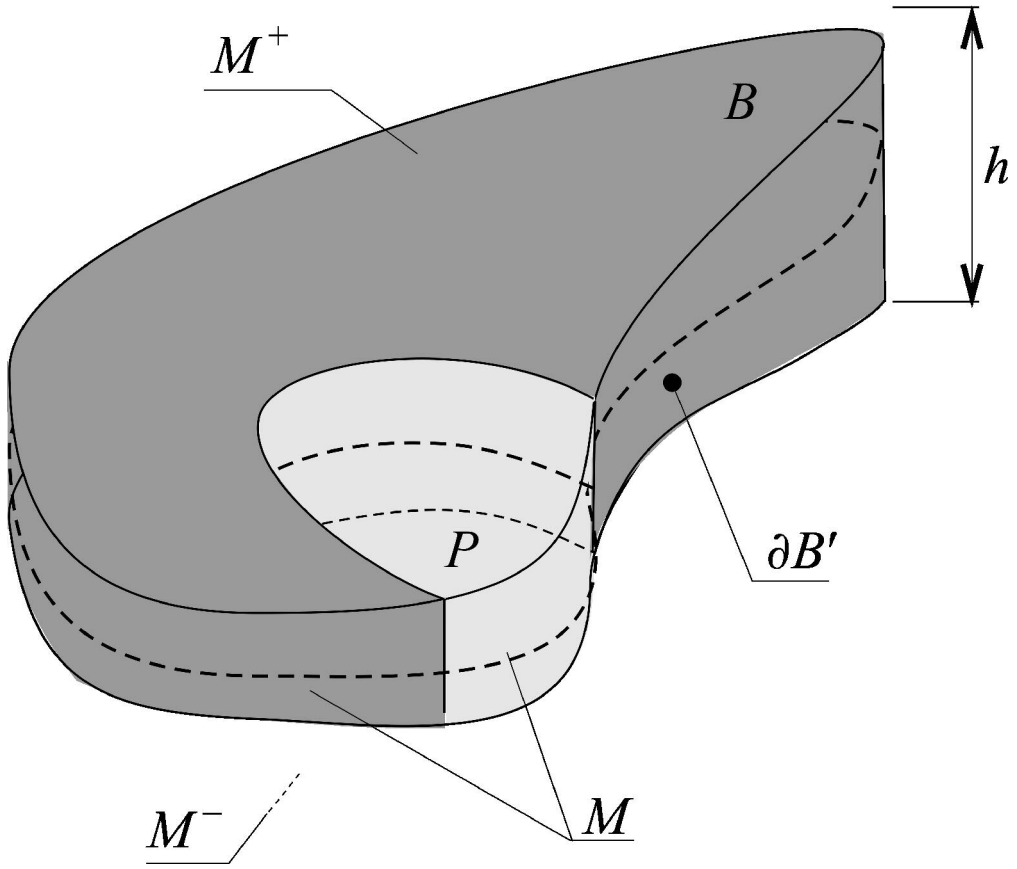

Figure 1. The shell-like body

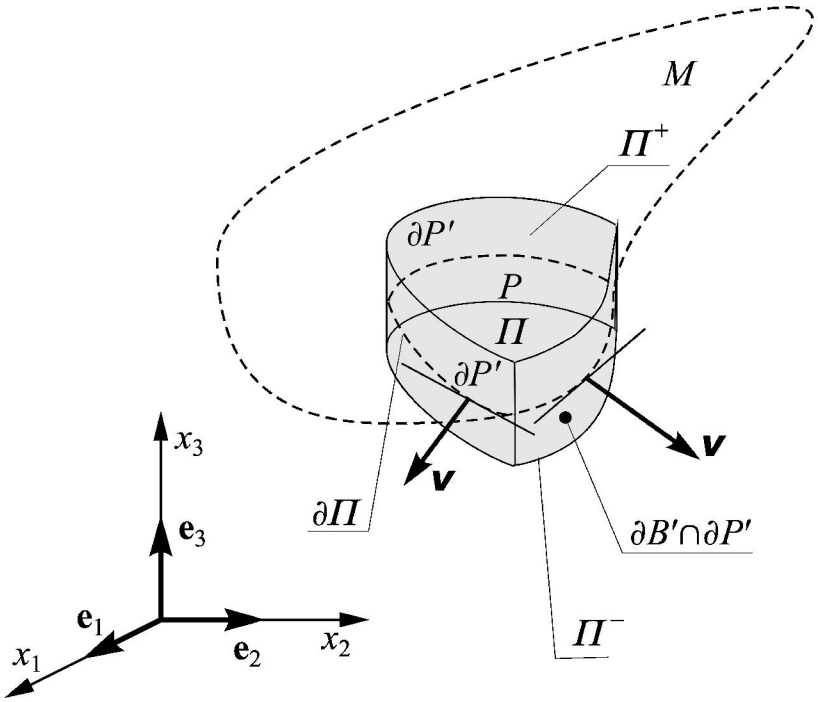

Figure 2. An arbitrary part of the shell-like body in the reference configuration

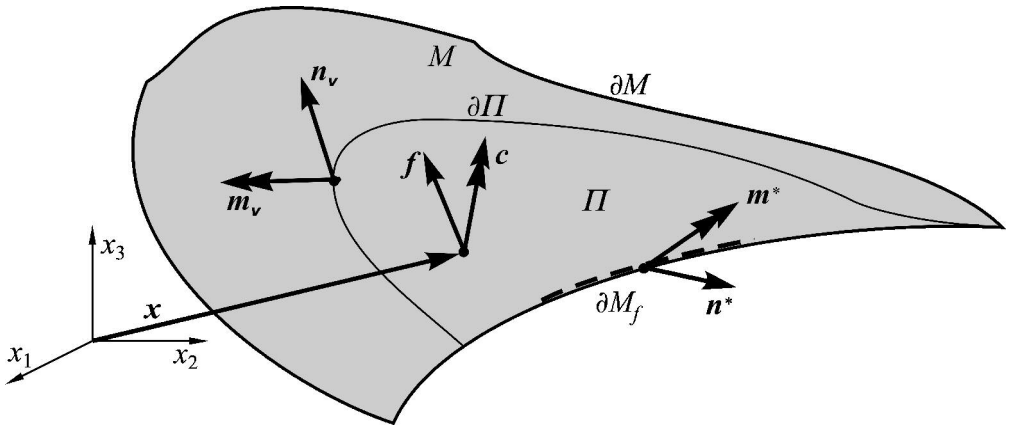

Figure 3. Resultant forces and couples

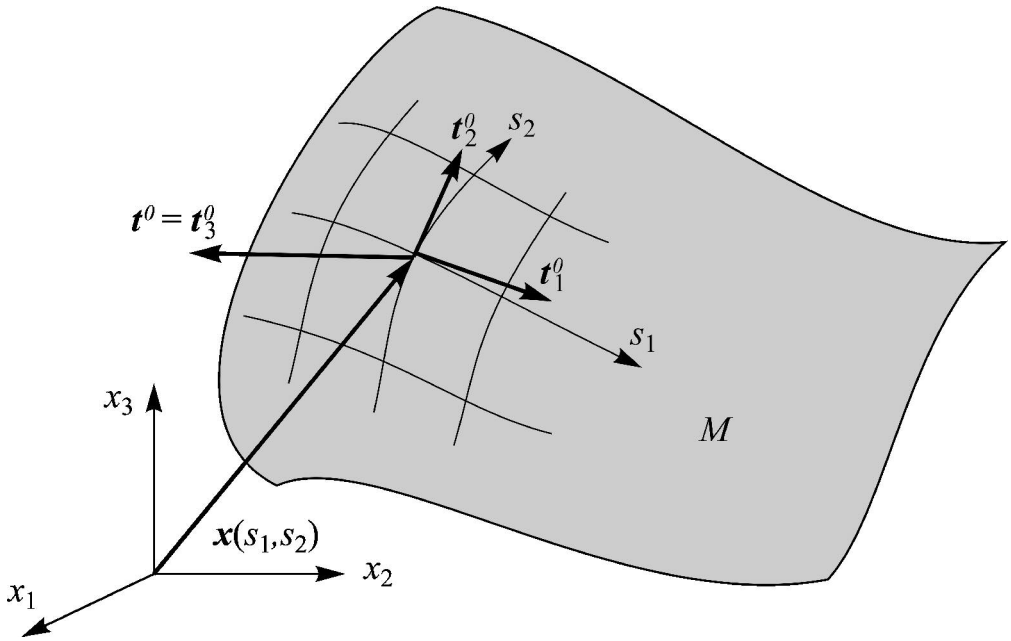

Figure 4. Formal, local, parametrization of M

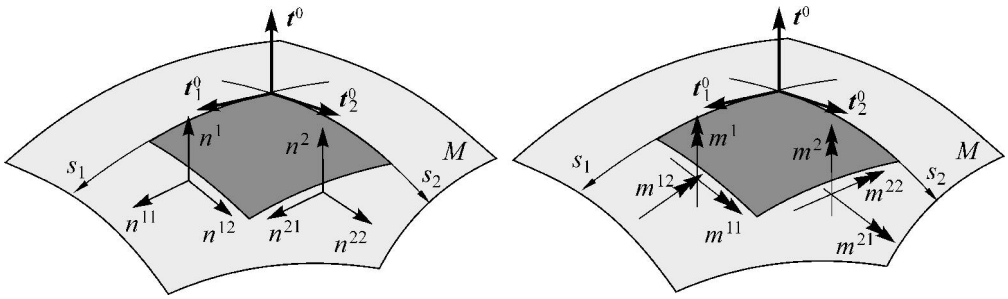

Figure 5. Physical components of resultant forces and moments

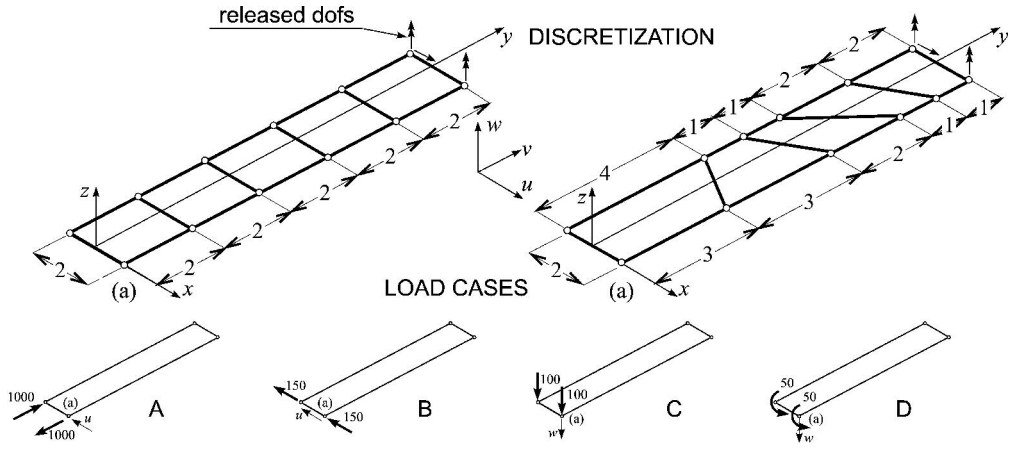

Figure 6. Partially clamped cantilever membrane/plate: geometry, load, discretizations

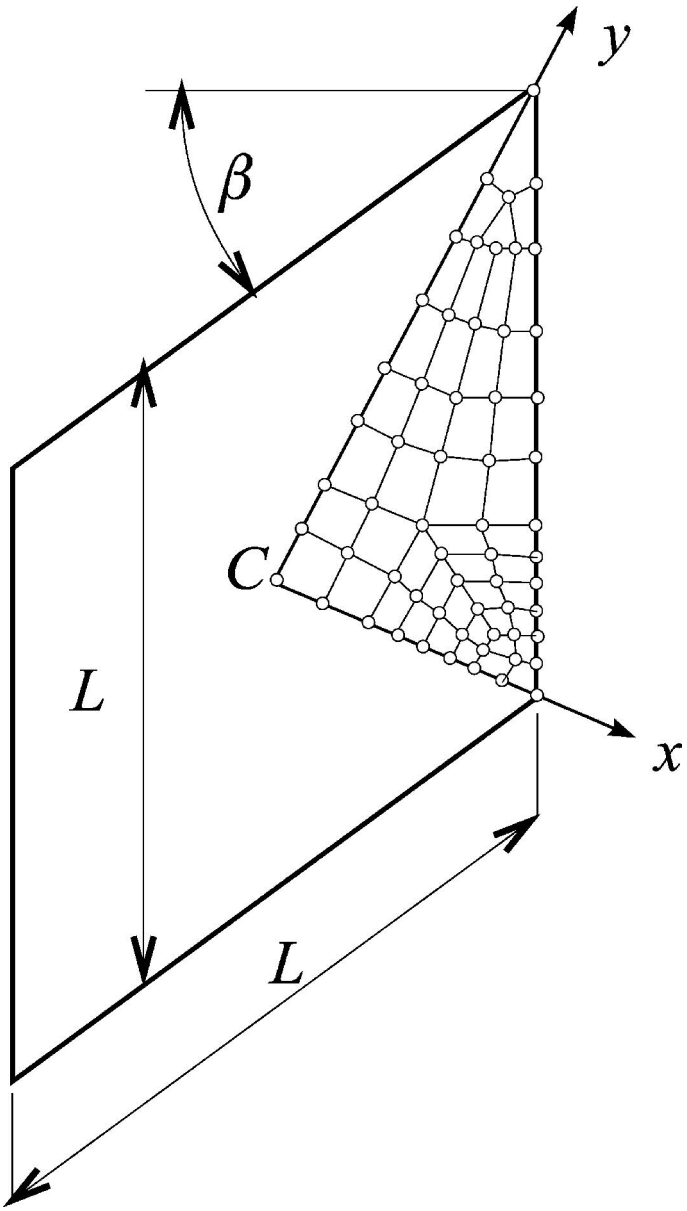

Figure 7. Clamped skew plate: geometry, discretization

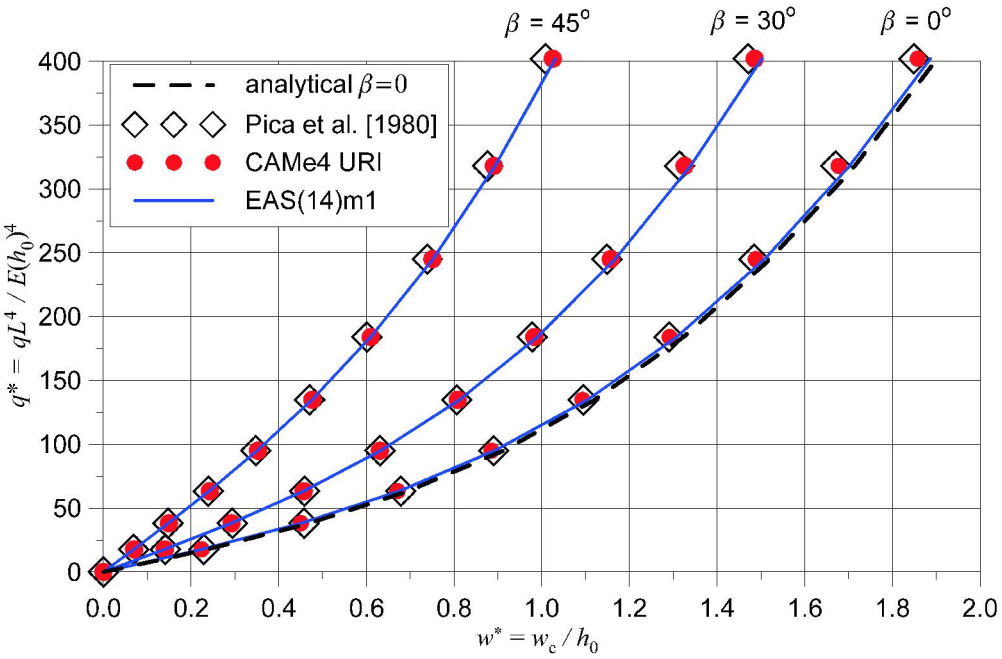

Figure 8. Clamped skew plate: load-displacement paths

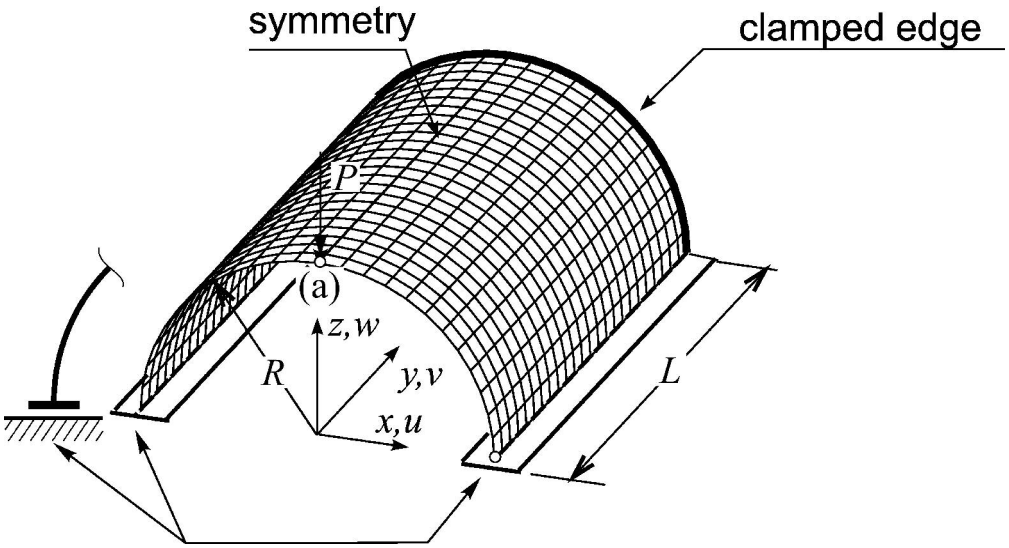

Figure 9. Pinched cylinder: geometry and load

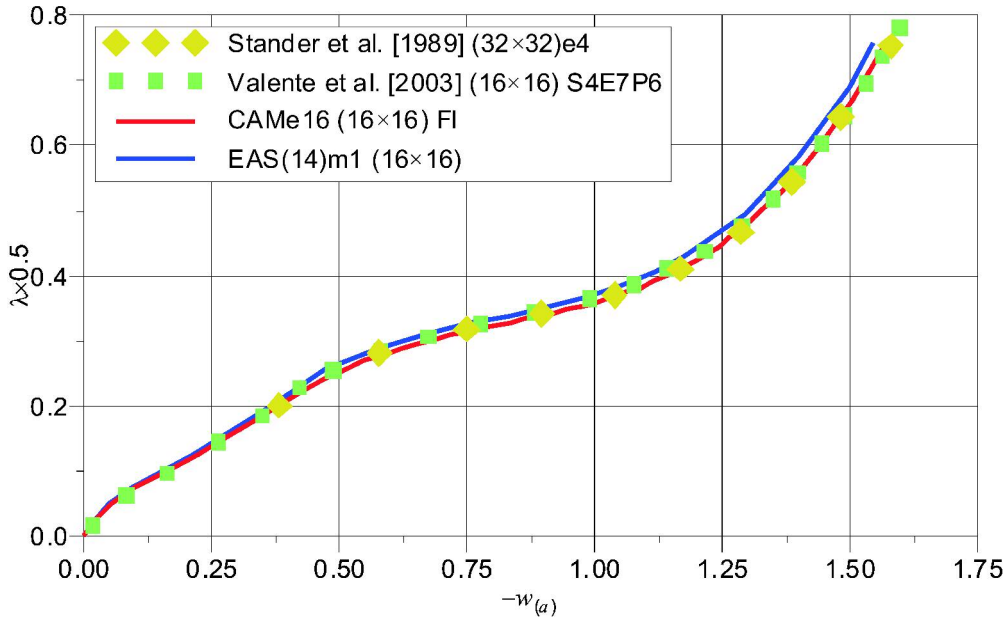

Figure 10. Pinched cylinder: load-displacement paths

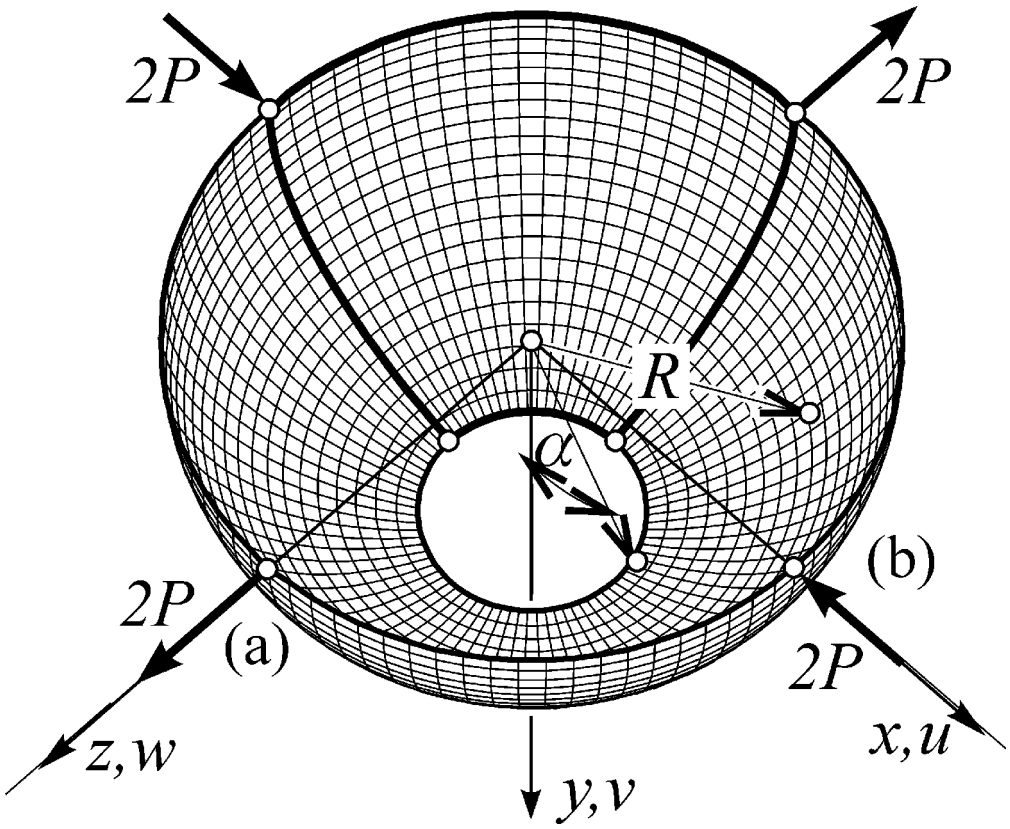

Figure 11. Pinched hemisphere with a hole: geometry and loads

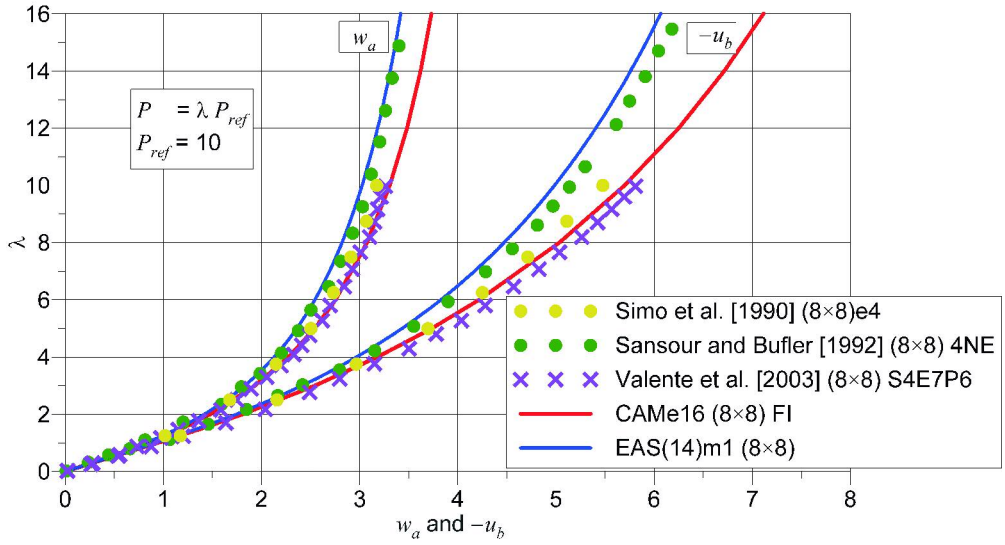

Figure 12. Pinched hemisphere: load-displacement paths, mesh 8x8

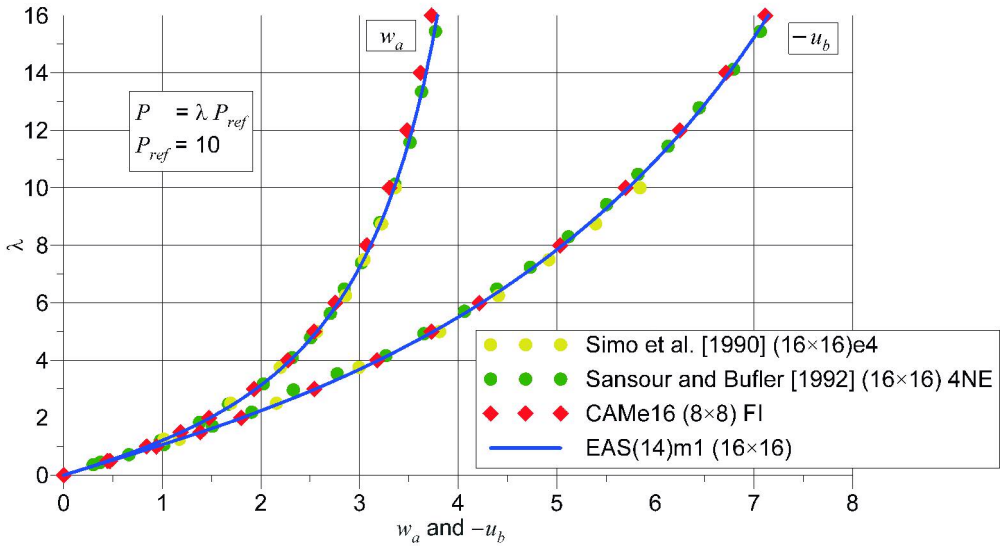

Figure 13. Pinched hemisphere: load-displacement paths, mesh 16x16

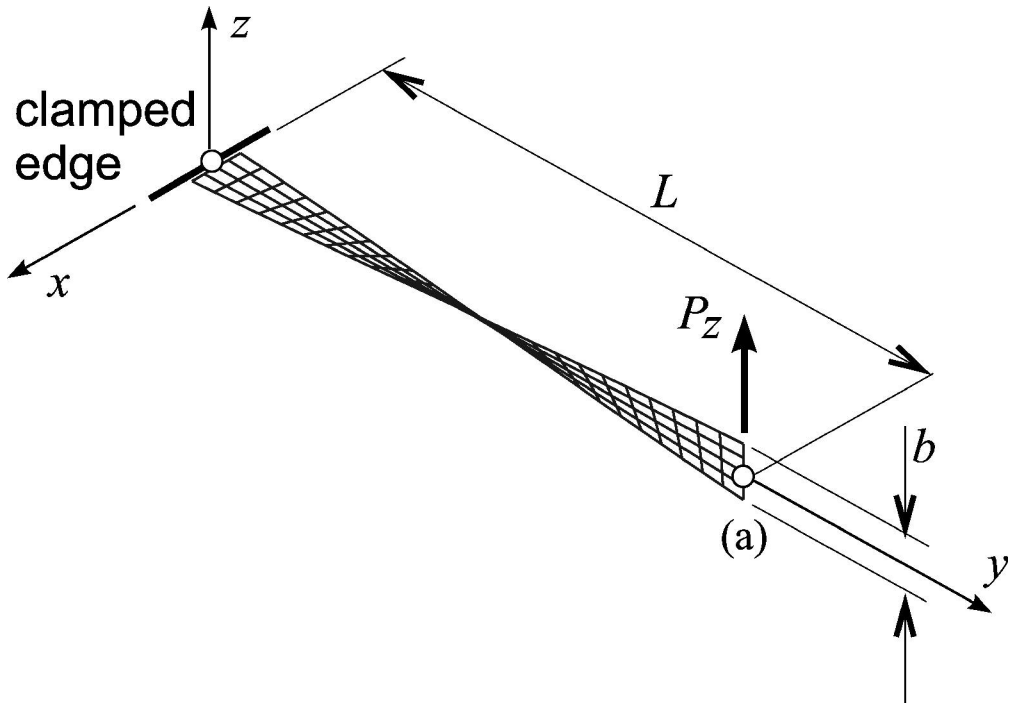

Figure 14. Twisted beam, geometry, loads

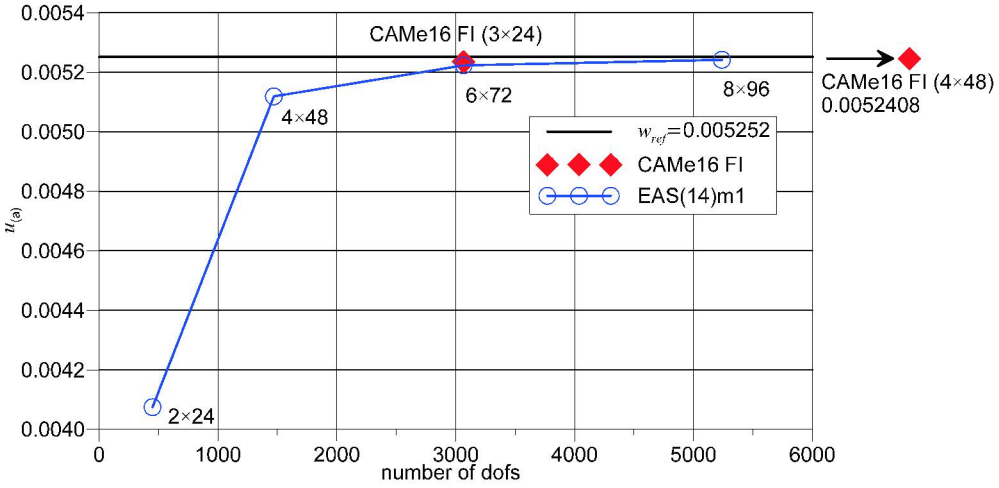

Figure 15. Twisted beam: linear convergence analysis

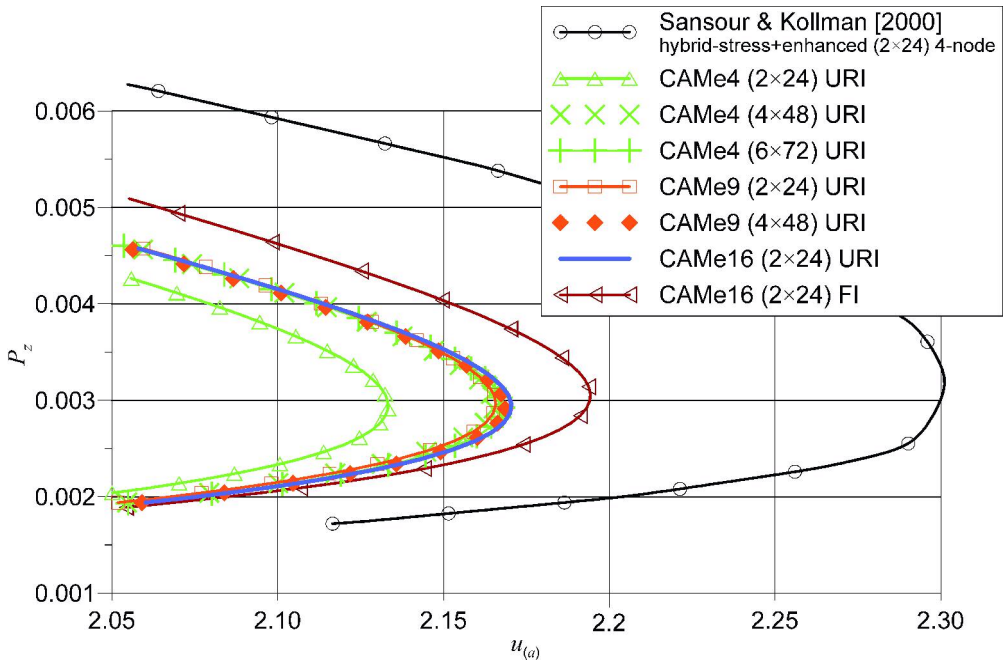

Figure 16. Twisted beam: nonlinear convergence analysis, CAM elements

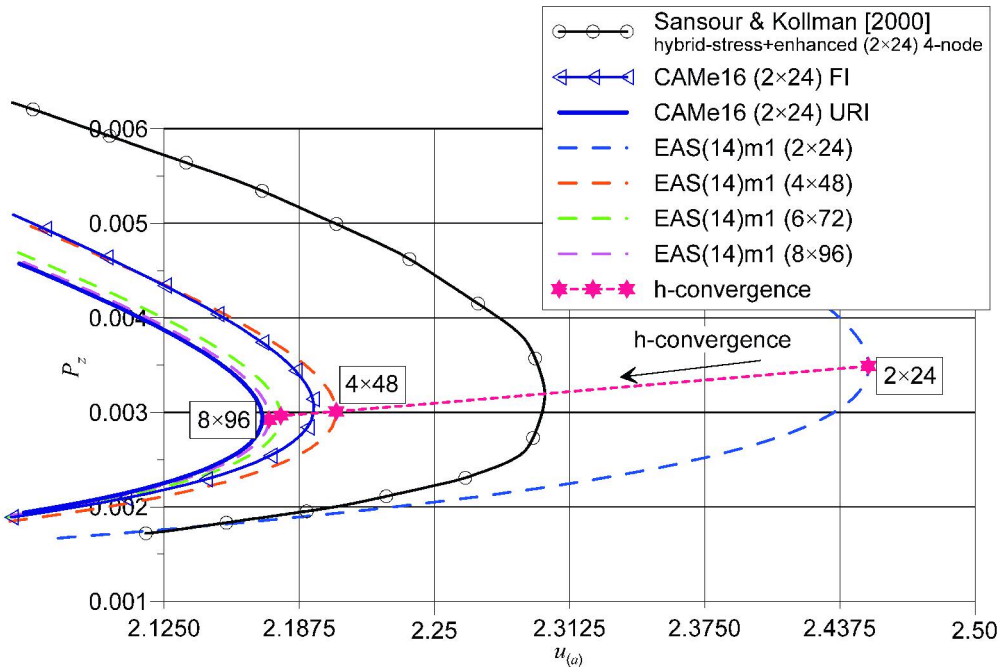

Figure 17. Twisted beam: nonlinear convergence analysis, EAS element

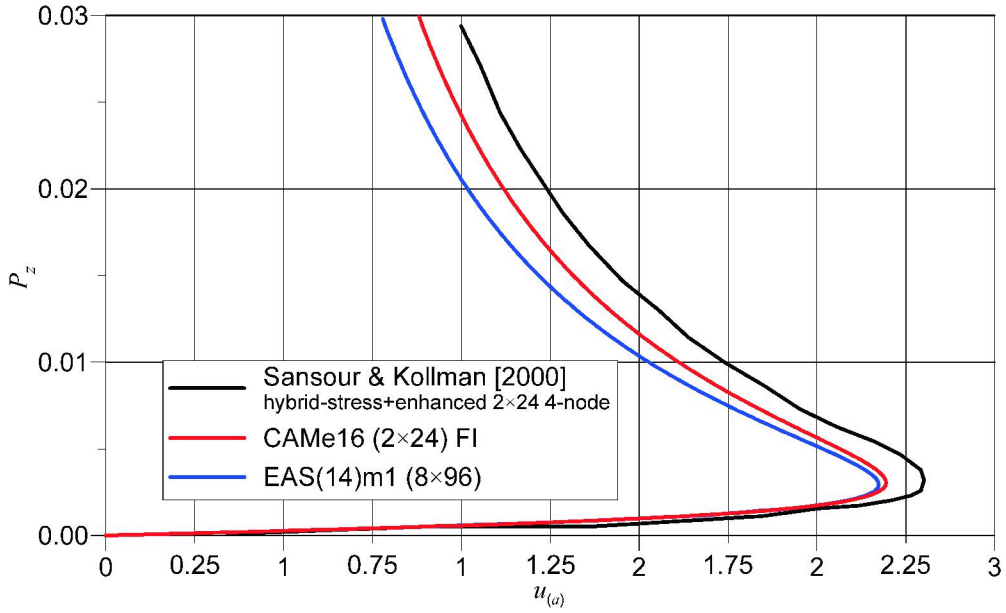

Figure 18. Twisted beam: nonlinear solution

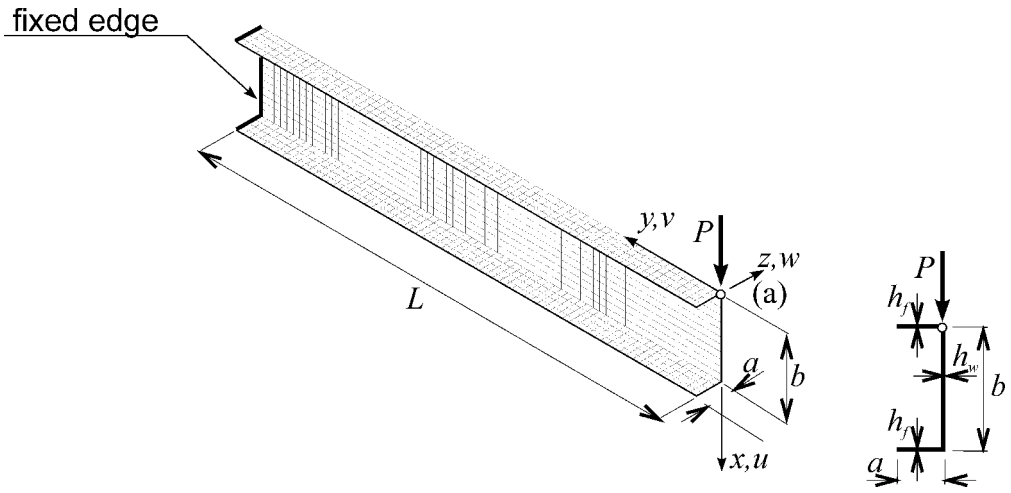

Figure 19. Channel section cantilever: geometry, load

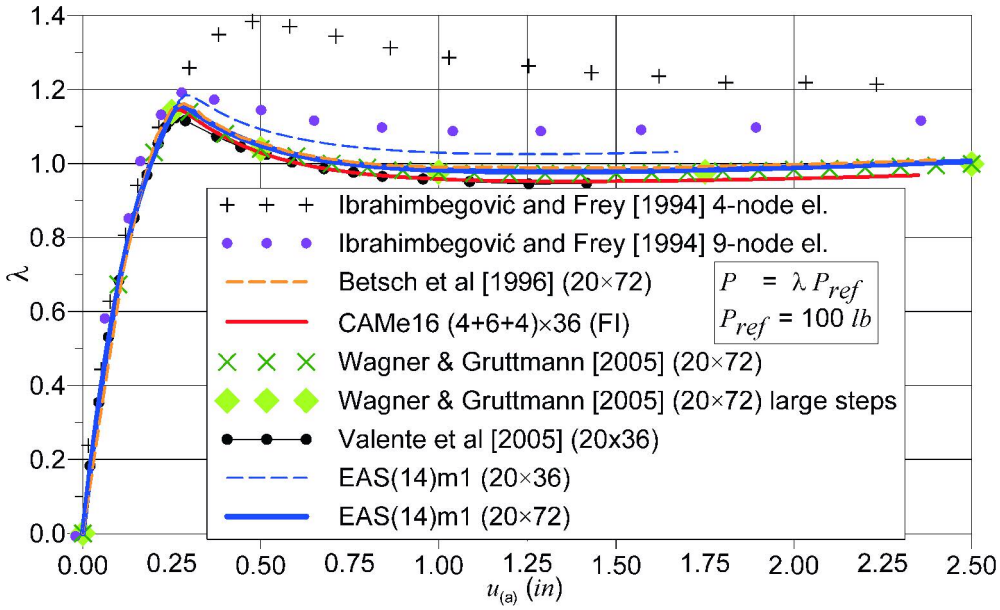

Figure 20. Channel section cantilever: variant 1, load-displacement paths

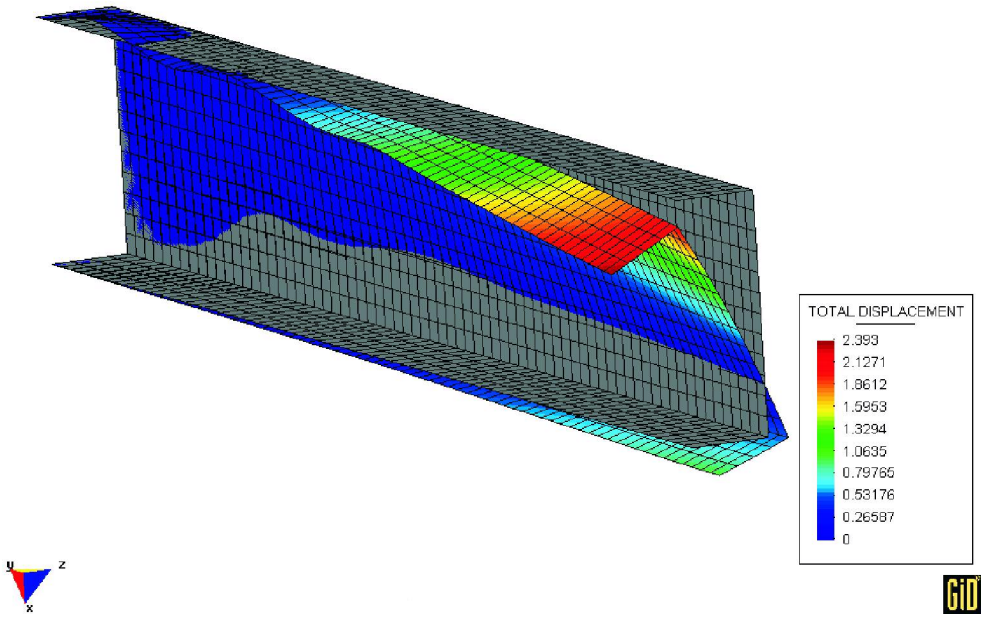

Figure 21. Channel section cantilever: variant 1, deformed configuration $\lambda = 1.01397$

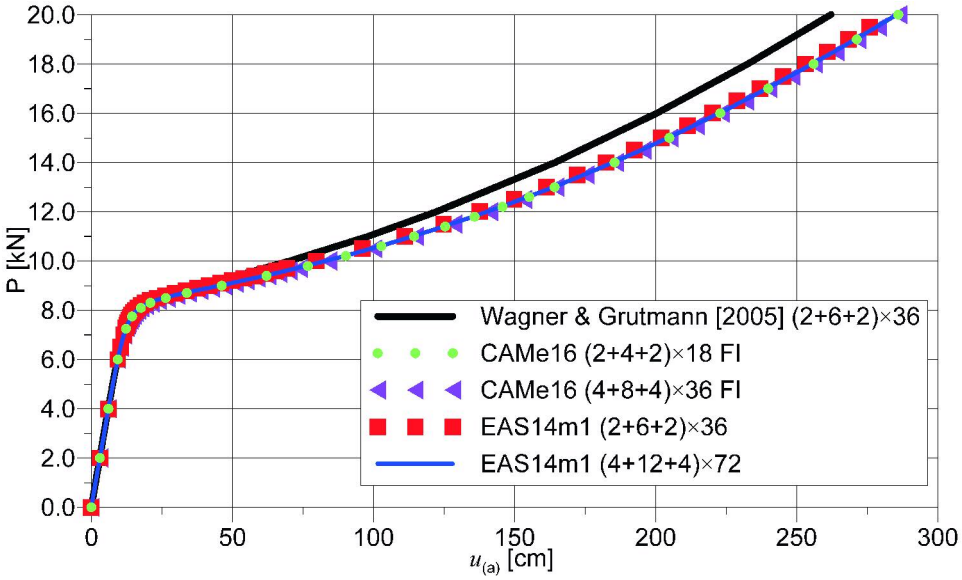

Figure 22. Channel section cantilever: variant 2, load-displacement paths

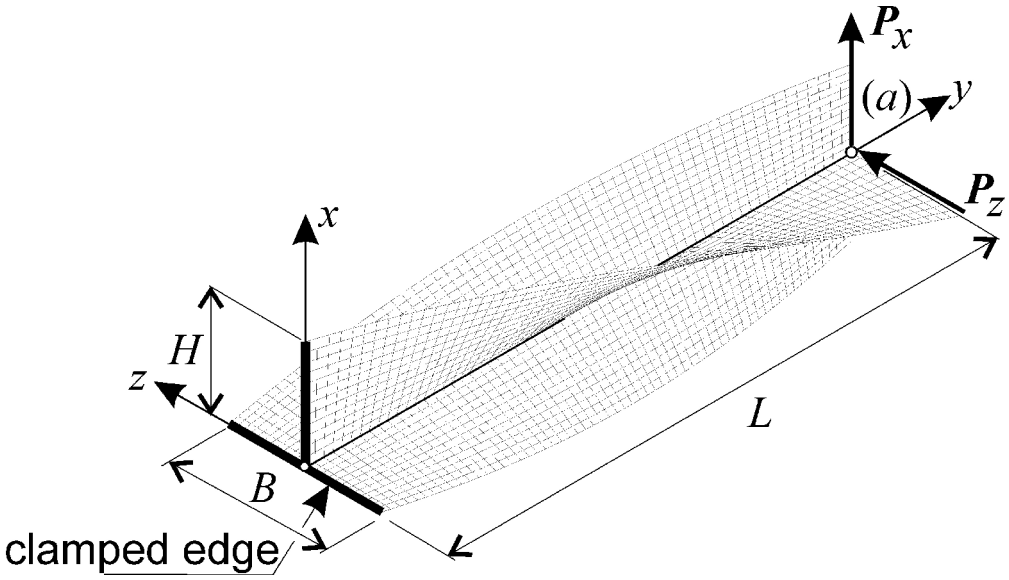

Figure 23. Twisted beam: geometry and loads

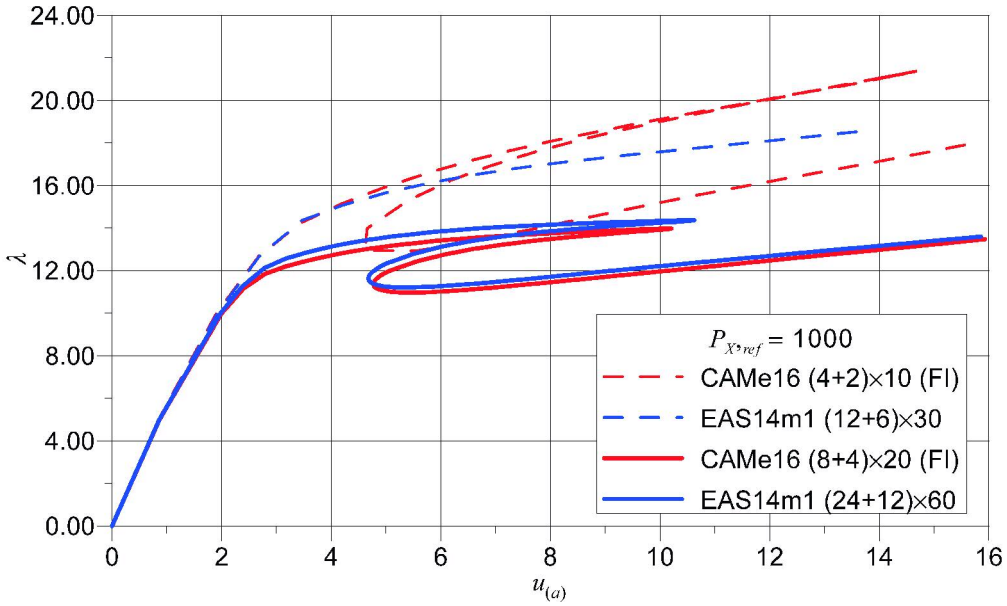

Figure 24. Twisted beam: nonlinear solutions

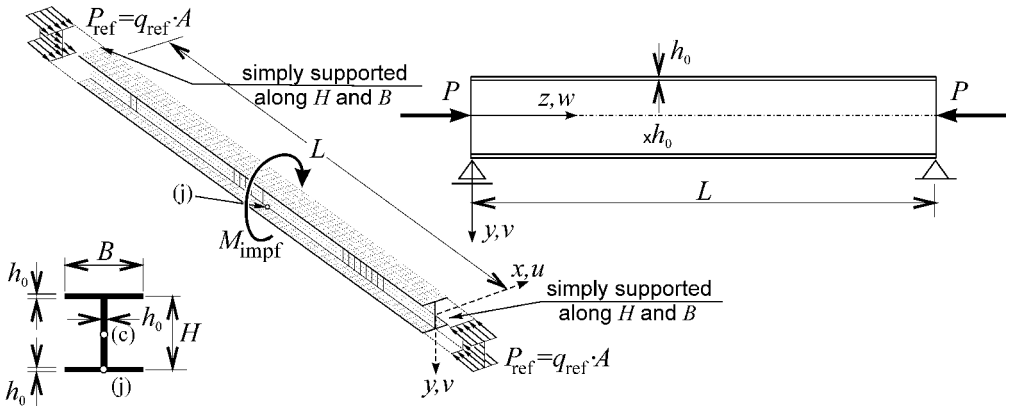

Figure 25. I-beam column: geometry and loads